Outage Probability Analysis of Spectrum Sharing Systems With Distributed Cyclic Delay Diversity

Kyeong Jin Kim, Hongwu Liu, Miaowen Wen, Marco Di Renzo, H. Vincent Poor

Outage Probability Analysis of Spectrum Sharing Systems with Distributed Cyclic Delay Diversity

Kyeong Jin Kim, Hongwu Liu, Miaowen Wen, Marco Di Renzo, and H. Vincent Poor

Abstract

In this paper, a distributed cognitive underlay single carrier system is investigated. A secondary users' network consists of a control unit (CU) and a group of secondary user remote radio heads (S-RRHs). To effectively access the radio spectrum licensed to the primary users, a distributed cyclic delay diversity (dCDD) scheme is employed between the CU and S-RRHs as the transmit diversity scheme. Multiple primary user transmitters (PTXs) are assumed to be located isotropically within the secondary users' network, so that a mixture of line-of-sight (LoS) and non-line-of-sight (nLoS) paths from the PTXs to the secondary user receiver is considered. In addition, a mixture of LoS and nLoS paths is considered in the secondary users' network. For a new transmit diversity scheme and channel model, the performance of the secondary users' network achieved by dCDD in the presence of isotropically distributed multiple PTXs is investigated. dCDD enables the CU to use multiple S-RRHs at the same time, so that determining the effects of a different number of S-RRHs in the presence of a new channel model is an open research issue. To this end, a new closed-form expression for the outage probability is derived, and then its accuracy is verified by link-level simulations.

Index Terms

Distributed cyclic delay diversity, underlay spectrum sharing, cyclic-prefixed single carrier transmission, outage probability, diversity gain.

I. Introduction

Since the radio frequency spectrum is a scarce natural resource, it needs to be efficiently utilized by all entities that want to use it. To mitigate its inefficient utilization, cognitive radio has been proposed by [2]. Among several approaches of cognitive radios, such as overlay, interweave, and underlay, underlay spectrum sharing is the most

K. J. Kim is with Mitsubishi Electric Research Laboratories (MERL), Cambridge, MA, 02139 USA (e-mail: kyeong.j.kim@hotmail.com).

H. Liu is with the School of Information Science and Electric Engineering, Shandong Jiaotong University, Jinan 250357, China (e-mail:hong.w.liu@hotmail.com).

M. Wen is with the School of Electronic and Information Engineering, South China University of Technology, Guangzhou 510641, China (e-mail:eemwwen@scut.edu.cn).

M. D. Renzo is with the Laboratoire des Signaux et Systèmes, CNRS, CentraleSupélec, Univ Paris Sud, Université Paris-Saclay, 3 rue Joliot Curie, Plateau du Moulon, 91192, Gif-sur-Yvette, France (e-mail:marco.direnzo@l2s.centralesupelec.fr).

H. V. Poor is with the Department of Electrical Engineering, Princeton University, Princeton, NJ, 08544 USA (e-mail:poor@princeton.edu).

Parts of this paper were presented at the 2018 Global Communications Conference [1].

promising since unlicensed secondary users can reuse the spectrum licensed to primary users in transmitting their information. As long as the aggregated received energy level from the secondary users' transmissions does not exceed an interference temperature limit at the primary users, the secondary users can use the licensed band.

To improve the performance of underlay spectrum sharing, several approaches have been proposed. Maximum ratio transmission (MRT) was proposed as a transmit diversity scheme by [3] for a transmitter deployed with multiple antennas. Recently, MRT has been applied to distributed single carrier transmission systems [4]. However, acquiring exact channel state information at the transmitter side (CSIT) is a challenging task in distributed wireless communications systems, in which transmit diversity heavily relies on CSIT.

As an alternative scheme, transmit antenna selection (TAS) has been proposed by [5]–[8] when multiple antennas are deployed at the single transmitter. Considering feedback overhead and signal processing cost, a single transmit antenna is selected in TAS to maximize the signal-to-noise ratio (SNR) at the secondary user receiver (SRX). In addition, a general maximal ratio combining (MRC) is applied among several receive antennas to enhance the performance of the secondary users' network. In particular, the ergodic capacity was investigated for TAS and MRC schemes in [5]. For multiple primary user receivers (PRXs) in the network, the outage probability of TAS and MRC schemes was investigated by [6]. The authors of [7] investigated the power allocation problem for TAS and MRC schemes with a single primary user transmitter (PTX) and PRX. Recently, the authors of [8] considered both continuous and discrete power adaptation to reduce the interference at the PRX.

With the aid of backhaul signaling, a decentralized multi-cell beamforming scheme was investigated in underlay spectrum sharing environments in [9]. Under ideal backhaul connections, joint information and energy cooperation between the primary and secondary systems was considered to improve the spectral efficiency for cognitive radio networks in [10]. In [11], the outage probability and ergodic capacity were investigated for best user selection in cognitive relay networks with unreliable backhaul connecting multiple users. To support several secondary base stations (SBSs) for simultaneous transmissions, precoding was proposed by [12] over the backhaul links between the control unit (CU) and SBSs.

In contrast to MRT, TAS, and the work [11] which applies best user selection to achieve transmit diversity, a distributed cyclic delay diversity (dCDD) has been proposed as a practical transmit diversity scheme for cyclic-prefixed single carrier (CP-SC) systems [13]. The dCDD scheme improves the reliability of a message by transmitting the same message over multiple channels having different channel characteristics. Although the dCDD protocol is similar to TAS in avoiding explicit channel feedback from the receiver, dCDD works effectively for distributed systems, in which only one antenna is deployed for each of the transmitters. In contrast, TAS assumes multiple transmit antennas deployed at a single transmitter, and thus how to use TAS in a distributed system is still an open problem. In addition, TAS supports only one antenna at each time epoch for transmission. In contrast, dCDD can use as many transmitters allowed by a frequency selective fading channel. Consequently, the dCDD protocol results in a higher coding gain while maintaining the same maximum diversity gain as TAS by intrinsically integrating opportunistic transmitter cooperation.

Several works [14]–[17] have applied the conventional CDD to different applications that use a cyclic delay among antennas deployed at a single transmitter. Accordingly, the conventional CDD scheme does not apply a cyclic

delay among multiple distributed antennas, each of which is deployed at a different spatially located transmitter in distributed systems. The authors of [13] firstly verified that by a proper design of the permutation matrix that circularly shifts the transmission symbol block, an intersymbol interference (ISI)-free channel matrix can be generated for distributed CP-SC transmissions. The size of the transmission symbol block which is specified by the CU based on the CP-SC transmissions, and the maximum number of multipath components of the channel that transmits this symbol block determine the number of transmitters for dCDD. The receiver needs to feedback the maximum number of multipath components to the CU. It has been verified by [13] that the full diversity gain with a higher coding gain can be achieved with respect to [18] and [19] without exact knowledge of CSIT. This performance gain advantage will be beneficial to secondary users in reusing the radio band licensed to primary users.

There are several existing works [20]–[22] on spectrum sharing systems that use CP-SC transmissions. In [20], the decode-and-forward relaying protocol and selection combining were employed. The joint impact of multiple licensed transceivers was investigated in [21]. Full-duplex relaying was studied in [22]. After proposing the CP-SC based spectrum sharing in [23], these works have verified that the multipath gain can be attained over frequency selective fading channels by proper use of the cyclic prefix and a very reliable data detector.

In contrast to existing works, our main contributions can be summarized as follows.

- To achieve the transmit diversity gain, dCDD is employed in the secondary users' network comprising the CU, a finite number of secondary user remote radio heads (S-RRHs), and a single SRX. Thus, we use a mathematical analysis fit to finite-sized cooperative spectrum sharing systems. Over a secondary users' network, we investigate the impact of the random location of multiple PTXs on the outage probability. Accordingly, the use of the dCDD protocol in the secondary users' network is one of the key distinctions from existing works, for example, [11] [12], [21], and [22].
- Due to the random location of the PTX within the secondary users' network, a more practical channel model, which is somewhat similar to that of [24]–[27], is used. The co-existence of line-of-sight (LoS) and non-line-of-sight (nLoS) paths is modeled by using a time-sharing factor [28], which is distributed as a Bernoulli process. However, we assume that a single PRX is placed at the location where the LoS path with respect to S-RRHs is dominating. Nevertheless, this assumption can be removed in performance analysis.
- We provide an analytical framework jointly taking into account a different degree of S-RRH cooperation via the dCDD protocol, non-identical frequency selective fading, random location of the PTX over co-existing LoS and nLoS paths, and coexisting LoS and nLoS paths over the secondary users' network. For this new system setting and channel model for the underlay spectrum sharing system, a new expression for the spatially averaged signal-to-interference ratio (SA-SIR) is derived.

A. Organization

The rest of the paper is organized as follows. In Section II, we detail the system and channel model of the dCDD-based CP-SC system. After defining random quantities and deriving their distributions, performance analysis of the

considered system in the interference limited regime is conducted in Section III. Simulation results are presented in Section IV and conclusions are drawn in Section V.

B. Notation

$\mathbb{N}_0$ denotes the set of non-negative integers; $\mathbb{C}$ denotes the set of complex numbers; $\boldsymbol{I}_N$ is the $N \times N$ identity matrix; $\mathbf{0}$ denotes an all-zero matrix of appropriate dimensions; $\mathcal{CN}\left(\mu, \sigma^2\right)$ denotes the circularly symmetric complex Gaussian distribution with mean μ and variance σ^2; $F_{\varphi}(\cdot)$ and $f_{\varphi}(\cdot)$, respectively, denote the cumulative distribution function (CDF) and probability density function (PDF) of the random variable (RV) φ; and $E\{\cdot\}$ denotes expectation. $\binom{n}{k} \triangleq \frac{n!}{(n-k)!k!}$ denotes the binomial coefficient. The lth element of a vector $\boldsymbol{a}$ is denoted by $\boldsymbol{a}(l)$; and $\mathbb{L}(\boldsymbol{a})$ denotes the cardinality of a vector $\boldsymbol{a}$. $\mathrm{RC}(\boldsymbol{a})$ denotes the right circulant matrix determined by column vector $\boldsymbol{a}$. $A|_{i\to j}$ denotes that a variable i in A is replaced by j. In specifying a channel related quantity, we use a consistent way as follows:

- $\boldsymbol{f}_{i,\mathrm{L}}$ denotes the ith vector of an f-type channel with the LoS path. Similarly, $\boldsymbol{F}_{i,\mathrm{L}}$ denotes the ith matrix of an f-type channel with the LoS path. The ith composite f-type channel vector from LoS and nLoS paths is denoted by $\boldsymbol{f}_i$.
- $N_{f,\mathrm{L}}$ denotes the number of multipath components of an f-type channel with the LoS path.
- $N_{f,\mathrm{L},m}$ denotes the number of multipath components of the mth f-type channel with the LoS path.
- Similar notations corresponding to the nLoS path can be specified.

In addition, subscripts are used to identify an element from a particular set.

II. System and Channel Model

Fig. 1 illustrates the considered dCDD-based spectrum sharing system comprising primary users' and secondary users' networks. As for the primary users' network, Q PTXs and a single PRX are assumed to be communicating via a dedicated and licensed radio frequency band. Only one antenna is assumed to be deployed at the primary and secondary users due to hardware and power constraints. A circular shaped communication cell of radius R for the secondary users is formed. In the cell, the locations of the Q PTXs are assumed to be isotropic, whereas the PRX is placed at a fixed location, $(x_{\mathrm{PRX}}, y_{\mathrm{PRX}})$. A plurality of M S-RRHs are distributed over the circumference of the cell. A secondary user network consisting of the CU, M S-RRHs, and SRX shares the primary users' licensed radio frequency band subject to interference constraints imposed by the PRX. Since dCDD adopts a distributed protocol, the CU specifies how to control M single antenna equipped S-RRHs [13] via dedicated highly reliable backhauls[1], $\{b_m\}_{m=1}^{M}$. The CU forms an information data being transmitted by S-RRHs simultaneously to the SRX by using dCDD, so that each S-RRH requires only a simple hardware and low transmission power to communicate with the SRX in achieving the transmit diversity gain in the frequency selective fading channel. A receiving unit for Global Navigation Satellite System (GNSS) (e.g., GPS, Galileo, Glonass, Quasi-Zenith Satellite System (QZSS), etc.) signal is deployed at the front-end of each node, so that S-RRHs can receive and transmit the same information

[1]In contrast to the works [4], [11], [12], a limited backhaul capacity and unreliable backhaul are not in the scope of this paper.

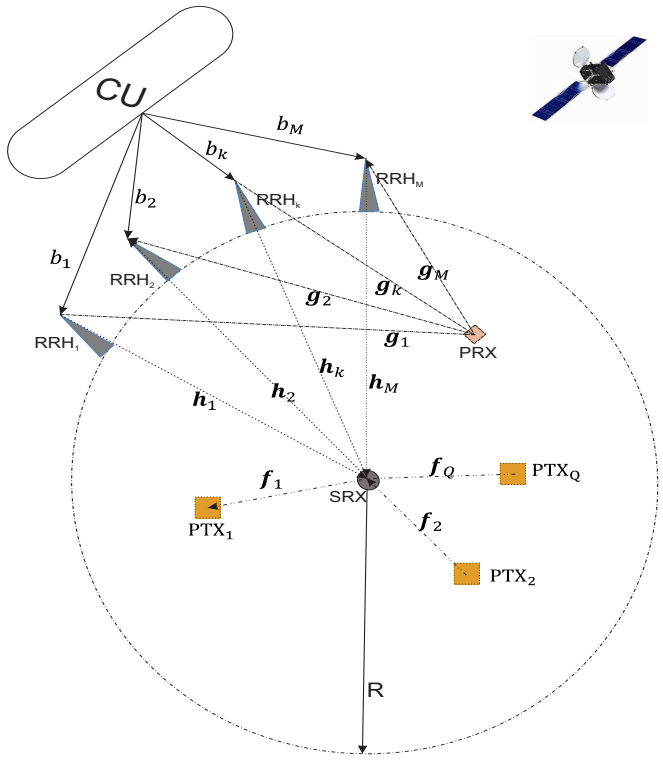

Fig. 1. Illustration of the considered dCDD-based spectrum sharing system with randomly located Q PTXs within the secondary users' cell.

data synchronously when they are operating for dCDD. Due to the use of half-duplex transceivers in every nodes, they are allowed to either send or receive data at a time.

Since the number of S-RRHs for dCDD is limited by the transmission symbol block size and the maximum multipath components over the frequency selective fading channel in the secondary users' network [13], this paper investigates only a finite-sized cooperative spectrum sharing system comprising a finite number of M S-RRHs and a single SRX for dCDD. By employing appropriate channel sounding schemes or channel reciprocity [29], [30], we further assume that the SRX is able to know the maximum number of multipath components over the channels from S-RRHs to itself. Note that dCDD has a very similar handshaking message overhead compared with TAS, wherein the receiving side conveys to the transmitting side the antenna index for transmissions. Since the considered system employs CP-SC transmissions, the SRX needs to convey the maximum number of multipath components over the channels from M S-RRHs to the SRX to the transmitting side to remove ISI. The following channels are assumed in the considered system.

- Channels from S-RRHs to the SRX: A multipath channel, $\boldsymbol{h}_m$, from the mth S-RRH to the SRX is given by[2]

$$\boldsymbol{h}_m = \mathbb{J}_{\mathrm{L}}\sqrt{(d_{1,m})^{-\epsilon_{\mathrm{L}}}}\tilde{\boldsymbol{h}}_{m,\mathrm{L}} + \mathbb{J}_{\mathrm{nL}}\sqrt{(d_{1,m})^{-\epsilon_{\mathrm{nL}}}}\tilde{\boldsymbol{h}}_{m,\mathrm{nL}} \tag{1}$$

[2]A similar model is also employed in [31] and [32]. Especially, a composite channel from LoS and nLoS paths is used for the ultra dense cloud small cell network by [31].

where $\tilde{\boldsymbol{h}}_{m,\mathrm{L}}$ and $\tilde{\boldsymbol{h}}_{m,\mathrm{nL}}$ identify the mth frequency selective fading channel connected to the mth S-RRH over LoS and nLoS paths with $N_{h,\mathrm{L},m} \triangleq \mathbb{L}(\tilde{\boldsymbol{h}}_{m,\mathrm{L}})$ and $N_{h,\mathrm{nL},m} \triangleq \mathbb{L}(\tilde{\boldsymbol{h}}_{m,\mathrm{nL}})$ multipath components. A distance from the mth S-RRH to the SRX is given by $d_{1,m}$ with $d_{1,m} = R, \forall m$, independent of the index of the S-RRH. In addition, ϵ_{L} and ϵ_{nL} are respectively denoting the path loss exponent of the LoS and nLoS paths. The indicator functions, $\mathbb{J}_{\mathrm{L}}$ and $\mathbb{J}_{\mathrm{nL}}$, model the random selection between LoS and nLoS paths with probability $P_r(\mathbb{J}_{\mathrm{L}}) = \mathcal{G}$ and $P_r(\mathbb{J}_{\mathrm{nL}}) = 1 - \mathcal{G}$, where $\mathcal{G}$ denotes the time-sharing factor [28]. The selection probability of LoS and nLoS paths is assumed to be identical over the channels from M S-RRHs to the SRX. In this paper, we model the random selection of LoS and nLoS paths using a Bernoulli process.

- Channel from the qth PTX to the SRX: A multipath channel from the PTX to the SRX is given by

$$\boldsymbol{f}_q = \mathbb{I}_{\mathrm{L}} \sqrt{(d_{2,q})^{-\epsilon_{\mathrm{L}}}} \tilde{\boldsymbol{f}}_{q,\mathrm{L}} + \mathbb{I}_{\mathrm{nL}} \sqrt{(d_{2,q})^{-\epsilon_{\mathrm{nL}}}} \tilde{\boldsymbol{f}}_{q,\mathrm{nL}} \tag{2}$$

where $\tilde{\boldsymbol{f}}_{q,\mathrm{L}}$ and $\tilde{\boldsymbol{f}}_{q,\mathrm{nL}}$ identify the qth frequency selective fading channel over LoS and nLoS paths with $N_{f,\mathrm{L}} \triangleq \mathbb{L}(\{\tilde{\boldsymbol{f}}_{q,\mathrm{L}}\}_{q=1}^{Q})$ and $N_{f,\mathrm{nL}} \triangleq \mathbb{L}(\{\tilde{\boldsymbol{f}}_{q,\mathrm{nL}}\}_{q=1}^{Q})$ multipath components. The indicator functions, $\mathbb{I}_{\mathrm{L}}$ and $\mathbb{I}_{\mathrm{nL}}$, are used to model the random selection of LoS and nLoS paths with probability $P_r(\mathbb{I}_{\mathrm{L}}) = \mathcal{F}$ and $P_r(\mathbb{I}_{\mathrm{nL}}) = 1 - \mathcal{F}$. The selection probability of LoS and nLoS paths is assumed to be identical over the channels from Q PTXs to the SRX. A Bernoulli process that models the selection of LoS and nLoS paths from the PTXs to the SRX is assumed to be independent of the Bernoulli process that models the selection of LoS and nLoS paths from S-RRHs to the SRX. With respect to the center of the communication cell, $d_2 = d_{2,q}, \forall q$, is distributed as follows:

$$f_{d_2}(y) = \frac{2y}{(R)^2 - (R_{\min})^2} \text{ for } R_{\min} \leq y \leq R. \tag{3}$$

When $d_2 < 1$, the received power level becomes larger than the transmit power [33], so that $R_{\min} \geq 1$.

- Channels from M S-RRHs to the PRX : When multiple S-RRHs are servicing for dCDD, they jointly influence the PRX. Accordingly, a channel from the mth S-RRH to the PRX is given by

$$\boldsymbol{g}_m = \sqrt{(d_{3,m})^{-\epsilon_{\mathrm{L}}}} \tilde{\boldsymbol{g}}_{m,\mathrm{L}} \tag{4}$$

where $\tilde{\boldsymbol{g}}_{m,\mathrm{L}}$ identifies the frequency selective fading channel with $N_g \triangleq \mathbb{L}(\{\tilde{\boldsymbol{g}}_{m,\mathrm{L}}\}_{m=1}^{M})$. A distance from the mth S-RRH to the PRX is given by $d_{3,m}$. From (4), we assume that channels from the S-RRHs to the PRX introduce only LoS path.

- A very reliable channel state information (CSI) from M S-RRHs to the PRX can be obtained via direct feedback from the PRX [34], indirect feedback from a band manager [35], and periodic pilot-aided sensing from the PRX [35].
- The multipath components of all the frequency selective fading channels are assumed to be independent and identically distributed (i.i.d.) according to $\mathcal{CN}(0, 1)$. However, due to different distances from the S-RRHs to the PRX, a composite frequency selective fading channel considering both small and large scale fading is distributed independently and non-identically distributed (i.n.i.d.) in the considered system. We also assume that all channels are constant over one data transmission interval due to a quasi-static channel assumption, but different from, and independent of those for other transmission intervals.

A. dCDD for CP-SC Transmissions

CP-SC transmissions [18] are used for all nodes in the primary and secondary users' networks. Since dCDD allows a plurality of S-RRHs to transmit the same block symbol block $\boldsymbol{s}$ at the same time, it is necessary to remove a possible existence of ISI at the SRX. In addition, due to operation in the multipath fading channel, ISI can be caused at the SRX. ISI being caused by a multipath channel can be removed by appending the last N_{CP}, which is called the CP length, symbols of $\boldsymbol{s} \in \mathbb{C}^{B\times 1}$ to the front of $\boldsymbol{s}$ [13]. The size of symbol block $\boldsymbol{s}$ is denoted by B. We assume that $E\{\boldsymbol{s}\} = \boldsymbol{0}$ and $E\{\boldsymbol{s}\boldsymbol{s}^H\} = \boldsymbol{I}_B$. Secondary, it is necessary to achieve the ISI-free reception at the SRX even for distributed joint CP-SC transmissions made by the synchronized S-RRHs. When the CU has knowledge about the CP length across the channels from the S-RRHs to the SRX, this can be possible by applying a different CDD delay, as a function of N_{CP}, to each of the S-RRHs. Let N_{CP} be defined by the maximum number of multipath components across the channels from the S-RRHs to the SRX, then the CDD delay, for example, the mth CDD delay, Δ_m, plays key roles in generating an equivalent ISI-free right circulant channel matrix by satisfying the following two conditions [13]:

$$N_{CP} \geq \max(N_{h,\mathrm{L},m}, N_{h,\mathrm{nL},m}) \text{ and } \Delta_m = (m-1)N_{CP}. \tag{5}$$

Note that when a mapping which assigns Δ_m to a particular S-RRH is shared among the nodes in the secondary user's network, this does not cause any performance differences. This is the one of the unique features of dCDD which was verified by [13]. For example, Eq. (5) specifies a linear mapping.

To make ISI free reception at the SRX from simultaneous distributed CP-SC transmissions, the CU determines the maximum allowable number of S-RRHs for dCDD as follows: $K = \lfloor B/N_{CP} \rfloor$, where $\lfloor \cdot \rfloor$ denotes the floor function. In this paper, we assume that $M \leq K$. However, when $M > K$, the SRX needs to convey a referencing order list of S-RRHs in accordance with the receive channel gain at the SRX, which enables the CU to choose only K S-RRHs for dCDD operation.

Having applied dCDD with the condition of $M \leq K$, the received signal at the SRX, after removing the CP signal, is given by

$$\begin{aligned} \boldsymbol{r} &= \sqrt{P_s}\sum_{m=1}^{M}\left(\mathbb{J}_{\mathrm{L}}(R)^{-\epsilon_{\mathrm{L}}/2}\tilde{\boldsymbol{H}}_{m,\mathrm{L}} + \mathbb{J}_{\mathrm{nL}}(R)^{-\epsilon_{\mathrm{nL}}/2}\tilde{\boldsymbol{H}}_{m,\mathrm{nL}}\right)\tilde{\boldsymbol{s}}_m + \\ &\quad \sqrt{P_P}\sum_{q=1}^{Q}\left(\mathbb{I}_{\mathrm{L}}(d_{2,q})^{-\epsilon_{\mathrm{L}}/2}\tilde{\boldsymbol{F}}_{q,\mathrm{L}} + \mathbb{I}_{\mathrm{nL}}(d_{2,q})^{-\epsilon_{\mathrm{nL}}/2}\tilde{\boldsymbol{F}}_{q,\mathrm{nL}}\right)\tilde{\boldsymbol{x}}_{q,p} + \boldsymbol{z}_R \end{aligned} \tag{6}$$

where $\tilde{\boldsymbol{s}}_m \triangleq \boldsymbol{P}_{\Delta_m}\boldsymbol{s}$ and P_P is the transmission power at the PTX. The additive noise over all the frequency selective fading channels is denoted by $\boldsymbol{z}_R \sim \mathcal{CN}(\boldsymbol{0}, \sigma_z^2\boldsymbol{I}_B)$. The permutation shifting matrix $\boldsymbol{P}_{\Delta_m}$ is obtained from the identity matrix $\boldsymbol{I}_B$ by circularly shifting down by Δ_m. Note that a set of S-RRHs can be recognized as a distributed antenna system with additional hardware resource, in which each S-RRH applies a simple operation, i.e., multiplying the permutation matrix $\boldsymbol{P}_{\Delta_m}$ to the incoming block symbol $\boldsymbol{s}$. After appending the last N_{CP} symbols of the transformed block symbol, each S-RRH transmits the resulting block symbol sequentially via its dedicated antenna.

As one example of dCDD operation, let us assume $B = 6$ and $N_{h,\mathrm{L},m} = 2, \forall m$, so that we have $N_{CP} = 2$ and $K = 3$. Furthermore, only two S-RRHs are available in the secondary users' network. Then, according to these assumptions, one particular channel matrix in (6) is defined by

$$
\begin{aligned}
(R)^{-\epsilon_{\mathrm{L}}/2}\tilde{\boldsymbol{H}}_{1,\mathrm{L}} &\triangleq (R)^{-\epsilon_{\mathrm{L}}/2}\begin{bmatrix}
\tilde{\boldsymbol{h}}_{1,\mathrm{L}}(1) & 0 & 0 & 0 & 0 & \tilde{\boldsymbol{h}}_{1,\mathrm{L}}(2) \\
\tilde{\boldsymbol{h}}_{1,\mathrm{L}}(2) & \tilde{\boldsymbol{h}}_{1,\mathrm{L}}(1) & 0 & 0 & 0 & 0 \\
0 & \tilde{\boldsymbol{h}}_{1,\mathrm{L}}(2) & \tilde{\boldsymbol{h}}_{1,\mathrm{L}}(1) & 0 & 0 & 0 \\
0 & 0 & \tilde{\boldsymbol{h}}_{1,\mathrm{L}}(2) & \tilde{\boldsymbol{h}}_{1,\mathrm{L}}(1) & 0 & 0 \\
0 & 0 & 0 & \tilde{\boldsymbol{h}}_{1,\mathrm{L}}(2) & \tilde{\boldsymbol{h}}_{1,\mathrm{L}}(1) & 0 \\
0 & 0 & 0 & 0 & \tilde{\boldsymbol{h}}_{1,\mathrm{L}}(2) & \tilde{\boldsymbol{h}}_{1,\mathrm{L}}(1)
\end{bmatrix} \\
&\triangleq (R)^{-\epsilon_{\mathrm{L}}/2}\mathrm{RC}\Big([(\tilde{\boldsymbol{h}}_{1,\mathrm{L}})^T,\ \boldsymbol{0}_{1\times 4}]^T\Big). \qquad (7)
\end{aligned}
$$

According to (7), $(R)^{-\epsilon_{\mathrm{nL}}/2}\tilde{\boldsymbol{H}}_{1,\mathrm{nL}}$ can be expressed by $(R)^{-\epsilon_{\mathrm{nL}}/2}\tilde{\boldsymbol{H}}_{1,\mathrm{nL}} = (R)^{-\epsilon_{\mathrm{nL}}/2}\mathrm{RC}\Big([(\tilde{\boldsymbol{h}}_{1,\mathrm{nL}})^T,\ \boldsymbol{0}_{1\times 4}]^T\Big)$. Recall that $\tilde{\boldsymbol{h}}_{1,\mathrm{L}}(i)$ denotes the ith element of $\tilde{\boldsymbol{h}}_{1,\mathrm{L}}$. Based on (7) and applying the linear mapping, the desired signal part in (6) can be expressed as

$$
\begin{aligned}
\boldsymbol{r}_s &= \sqrt{P_s}\sum_{m=1}^{2}\Big(\mathbb{J}_{\mathrm{L}}(R)^{-\epsilon_{\mathrm{L}}/2}\tilde{\boldsymbol{H}}_{m,\mathrm{L}} + \mathbb{J}_{\mathrm{nL}}(R)^{-\epsilon_{\mathrm{nL}}/2}\tilde{\boldsymbol{H}}_{m,\mathrm{nL}}\Big)\boldsymbol{P}_{\Delta_m}\boldsymbol{s} \\
&= \sqrt{P_s}\sum_{m=1}^{2}\left[\mathbb{J}_{\mathrm{L}}(R)^{-\epsilon_{\mathrm{L}}/2}\mathrm{RC}\Big([(\tilde{\boldsymbol{h}}_{m,\mathrm{L}})^T,\ \boldsymbol{0}_{1\times 4}]^T\Big) + \mathbb{J}_{\mathrm{nL}}(R)^{-\epsilon_{\mathrm{nL}}/2}\mathrm{RC}\Big([(\tilde{\boldsymbol{h}}_{m,\mathrm{nL}})^T,\ \boldsymbol{0}_{1\times 4}]^T\Big)\right]\boldsymbol{P}_{\Delta_m}\boldsymbol{s} \\
&= \mathbb{J}_{\mathrm{L}}\sqrt{P_s}(R)^{-\epsilon_{\mathrm{L}}/2}\mathrm{RC}\Big([(\tilde{\boldsymbol{h}}_{1,\mathrm{L}})^T,(\tilde{\boldsymbol{h}}_{2,\mathrm{L}})^T,\boldsymbol{0}_{1\times 2}]^T\Big)\boldsymbol{s} + \\
&\qquad \mathbb{J}_{\mathrm{nL}}\sqrt{P_s}(R)^{-\epsilon_{\mathrm{nL}}/2}\mathrm{RC}\Big([(\tilde{\boldsymbol{h}}_{1,\mathrm{nL}})^T,(\tilde{\boldsymbol{h}}_{2,\mathrm{nL}})^T,\boldsymbol{0}_{1\times 2}]^T\Big)\boldsymbol{s} \\
&= \Big(\mathbb{J}_{\mathrm{L}}\sqrt{P_s}\tilde{\boldsymbol{H}}_{\mathrm{eq,L}} + \mathbb{J}_{\mathrm{nL}}\sqrt{P_s}\tilde{\boldsymbol{H}}_{\mathrm{eq,nL}}\Big)\boldsymbol{s}. \qquad (8)
\end{aligned}
$$

In (8), $\boldsymbol{P}_{\Delta_m}$ has six rows and columns, which are determined by the block size B. According to the representation provided in (7), $\tilde{\boldsymbol{H}}_{\mathrm{eq,L}}$ is given by

$$
\begin{aligned}
\tilde{\boldsymbol{H}}_{\mathrm{eq,L}} &\triangleq (R)^{-\epsilon_{\mathrm{L}}/2}\tilde{\boldsymbol{H}}_{1,\mathrm{L}}\boldsymbol{P}_{\Delta_1} + (R)^{-\epsilon_{\mathrm{L}}/2}\tilde{\boldsymbol{H}}_{2,\mathrm{L}}\boldsymbol{P}_{\Delta_2} \\
&= (R)^{-\epsilon_{\mathrm{L}}/2}\begin{bmatrix}
\tilde{\boldsymbol{h}}_{1,\mathrm{L}}(1) & 0 & 0 & \tilde{\boldsymbol{h}}_{2,\mathrm{L}}(2) & \tilde{\boldsymbol{h}}_{2,\mathrm{L}}(1) & \tilde{\boldsymbol{h}}_{1,\mathrm{L}}(2) \\
\tilde{\boldsymbol{h}}_{1,\mathrm{L}}(2) & \tilde{\boldsymbol{h}}_{1,\mathrm{L}}(1) & 0 & 0 & \tilde{\boldsymbol{h}}_{2,\mathrm{L}}(2) & \tilde{\boldsymbol{h}}_{2,\mathrm{L}}(1) \\
\tilde{\boldsymbol{h}}_{2,\mathrm{L}}(1) & \tilde{\boldsymbol{h}}_{1,\mathrm{L}}(2) & \tilde{\boldsymbol{h}}_{1,\mathrm{L}}(1) & 0 & 0 & \tilde{\boldsymbol{h}}_{2,\mathrm{L}}(2) \\
\tilde{\boldsymbol{h}}_{2,\mathrm{L}}(2) & \tilde{\boldsymbol{h}}_{2,\mathrm{L}}(1) & \tilde{\boldsymbol{h}}_{1,\mathrm{L}}(2) & \tilde{\boldsymbol{h}}_{1,\mathrm{L}}(1) & 0 & 0 \\
0 & \tilde{\boldsymbol{h}}_{2,\mathrm{L}}(2) & \tilde{\boldsymbol{h}}_{2,\mathrm{L}}(1) & \tilde{\boldsymbol{h}}_{1,\mathrm{L}}(2) & \tilde{\boldsymbol{h}}_{1,\mathrm{L}}(1) & 0 \\
0 & 0 & \tilde{\boldsymbol{h}}_{2,\mathrm{L}}(2) & \tilde{\boldsymbol{h}}_{2,\mathrm{L}}(1) & \tilde{\boldsymbol{h}}_{1,\mathrm{L}}(2) & \tilde{\boldsymbol{h}}_{1,\mathrm{L}}(1)
\end{bmatrix}. \qquad (9)
\end{aligned}
$$

Similarly, $\tilde{\boldsymbol{H}}_{\mathrm{eq,nL}}$ can be determined. From (9), we can readily see that frequency selectivity becomes more severe. However, ISI-free CP-SC transmissions can be possible by the use of dCDD. Thus, a frequency

diversity gain can be achieved by dCDD. In contrast, $\tilde{\boldsymbol{F}}_{q,\mathrm{L}}$ and $\tilde{\boldsymbol{F}}_{q,\mathrm{nL}}$ follow the form defined by (7), that is, $\tilde{\boldsymbol{F}}_{q,\mathrm{L}} = \mathrm{RC}\Big([(\tilde{\boldsymbol{f}}_{q,\mathrm{L}})^T, \boldsymbol{0}_{1\times(B-N_{q,\mathrm{L}})}]^T\Big)$ and $\tilde{\boldsymbol{F}}_{q,\mathrm{nL}} = \mathrm{RC}\Big([(\tilde{\boldsymbol{f}}_{q,\mathrm{nL}})^T, \boldsymbol{0}_{1\times(B-N_{q,\mathrm{nL}})}]^T\Big)$.

The transmission power at all the S-RRHs is P_s, which is given by the following constraint [21]:

$$P_s = \min\left(P_T, \frac{I_p}{\max\limits_{m=1,\ldots,M}(d_{3,m})^{-\epsilon_{\mathrm{L}}}\|\tilde{\boldsymbol{g}}_{m,\mathrm{L}}\|^2}\right) \tag{10}$$

where P_T and I_p respectively denote the maximum allowable transmission power at all the S-RRHs and the peak allowable interference temperature at the PRX. The distance from the mth S-RRH to the PRX is given by $d_{3,m}$. Since $\max\{N_{h,\mathrm{L},m}, N_{h,\mathrm{nL},m}, N_{f,\mathrm{L}}, N_{f,\mathrm{nL}}, N_g\}$ is smaller than the block size B, a zero padding is required in the representation of right circulant channel matrices, $\tilde{\boldsymbol{H}}_{m,\mathrm{L}}$, $\tilde{\boldsymbol{H}}_{m,\mathrm{nL}}$, $\tilde{\boldsymbol{F}}_{q,\mathrm{L}}$, and $\tilde{\boldsymbol{F}}_{q,\mathrm{nL}}$. Note that when $M > K$, the CU chooses only K S-RRHs having greater channel gains, so that the order statistics are implicitly assumed in the representation of equivalent channel matrices $\tilde{\boldsymbol{H}}_{\mathrm{eq,L}}$ and $\tilde{\boldsymbol{H}}_{\mathrm{eq,nL}}$. The transmission symbol block from the qth PTX is given by $\tilde{\boldsymbol{x}}_{q,p}$ with $E\{\tilde{\boldsymbol{x}}_{q,p}\} = \boldsymbol{0}, \forall q$ and $E\{\tilde{\boldsymbol{x}}_{q,p}(\tilde{\boldsymbol{x}}_{q',p})^H\} = \boldsymbol{I}_B\delta_{q-q'}$ with the Kronecker delta function, $\delta_l = \begin{cases}0 & \text{if } l \neq 0.\\ 1 & \text{if } l = 0\end{cases}$

III. Performance Analysis in Interference Limited Regime

From (6), the signal-to-interference ratio (SIR) measured at the SRX is given by

$$\gamma_{\text{SIR}} \triangleq \frac{P_s\Big(\mathbb{J}_{\mathrm{L}}\sum_{m=1}^{M}\alpha_{h,\mathrm{L}}\|\tilde{\boldsymbol{h}}_{m,\mathrm{L}}\|^2 + \mathbb{J}_{\mathrm{nL}}\sum_{m=1}^{M}\alpha_{h,\mathrm{nL}}\|\tilde{\boldsymbol{h}}_{m,\mathrm{nL}}\|^2\Big)}{P_P\Big(\sum_{q=1}^{Q}\mathbb{I}_{\mathrm{L}}(d_{2,q})^{-\epsilon_{\mathrm{L}}}\|\tilde{\boldsymbol{f}}_{q,\mathrm{L}}\|^2 + \sum_{q=1}^{Q}\mathbb{I}_{\mathrm{nL}}(d_{2,q})^{-\epsilon_{\mathrm{nL}}}\|\tilde{\boldsymbol{f}}_{q,\mathrm{nL}}\|^2\Big)} \tag{11}$$

where $\alpha_{h,\mathrm{L}} \triangleq (R)^{-\epsilon_{\mathrm{L}}}$ and $\alpha_{h,\mathrm{nL}} \triangleq (R)^{-\epsilon_{\mathrm{nL}}}$. Note that when we use a maximum likelihood type detector, for example, the QRD-M [36], we can obtain (11). Further exploiting synchronized communications by GNSS and independent interference from Q PTXs to the SRX, we can rewrite (11) as

$$\gamma_{\text{SIR}} \triangleq \frac{P_s\Big(\mathbb{J}_{\mathrm{L}}\sum_{m=1}^{M}\alpha_{h,\mathrm{L}}\|\tilde{\boldsymbol{h}}_{m,\mathrm{L}}\|^2 + \mathbb{J}_{\mathrm{nL}}\sum_{m=1}^{M}\alpha_{h,\mathrm{nL}}\|\tilde{\boldsymbol{h}}_{m,\mathrm{L}}\|^2\Big)}{P_P\Big(\mathbb{I}_{\mathrm{L}}(d_2)^{-\epsilon_{\mathrm{L}}}\|\tilde{\boldsymbol{f}}_{\mathrm{L}}\|^2 + \mathbb{I}_{\mathrm{nL}}(d_2)^{-\epsilon_{\mathrm{nL}}}\|\tilde{\boldsymbol{f}}_{\mathrm{nL}}\|^2\Big)} = \min\Big(P_T, I_p/X\Big)Y. \tag{12}$$

In (12), we have defined $X \triangleq \max\limits_{m=1,\ldots,M}P_G(d_{3,m})^{-\epsilon_{\mathrm{L}}}\|\tilde{\boldsymbol{g}}_m\|^2$, $Y \triangleq \frac{A_{\mathrm{L}}+A_{\mathrm{nL}}}{B}$ with $A_{\mathrm{L}} \triangleq \mathbb{J}_{\mathrm{L}}\sum_{m=1}^{M}\alpha_{h,\mathrm{L}}\|\tilde{\boldsymbol{h}}_{m,\mathrm{L}}\|^2$ and $A_{\mathrm{nL}} \triangleq \mathbb{J}_{\mathrm{nL}}\sum_{m=1}^{M}\alpha_{h,\mathrm{nL}}\|\tilde{\boldsymbol{h}}_{m,\mathrm{nL}}\|^2$, and $B \triangleq P_P\Big(\mathbb{I}_{\mathrm{L}}(d_2)^{-\epsilon_{\mathrm{L}}}\|\tilde{\boldsymbol{f}}_{\mathrm{L}}\|^2 + \mathbb{I}_{\mathrm{nL}}(d_2)^{-\epsilon_{\mathrm{nL}}}\|\tilde{\boldsymbol{f}}_{\mathrm{nL}}\|^2\Big)$ with $\tilde{\boldsymbol{f}}_{\mathrm{L}} \triangleq \sum_{q=1}^{Q}\tilde{\boldsymbol{f}}_{q,\mathrm{L}}$ and $\tilde{\boldsymbol{f}}_{\mathrm{nL}} \triangleq \sum_{q=1}^{Q}\tilde{\boldsymbol{f}}_{q,\mathrm{nL}}$. Note that (12) equals (11) in the SA sense.

A. Distributions of the SA-SIR

Owing to the random locations of Q PTXs within the secondary users' cell, we need to compute the SA-SIR. Moving from the analysis of [21], the CDF of the SA-SIR is given by

$$\begin{aligned}F_{\gamma_{\text{SIR}}}(x) &= E\{Pr(Y < x/P_T, X < \mu|d_2)\} + E\{Pr(Y < Xx/I_p, X > \mu|d_2)\}\\ &= E\{F_Y(x/P_T|d_2)\}F_X(\mu) + E\left\{\int_{\mu}^{\infty}F_Y(xt/I_p|d_2)\right\}f_X(t)dt\end{aligned}$$

$$= \underbrace{F_{Y,\mathrm{SA}}(x/P_T)F_X(\mu)}_{J_1} + \underbrace{\int_{\mu}^{\infty} F_{Y,\mathrm{SA}}(xt/I_p)f_X(t)\,dt}_{J_2} \tag{13}$$

where $\mu \triangleq \frac{I_p}{P_T}$.

1) Distribution of the RV X: According to [21], we can compute the distributions of RV X as follows:

$$F_X(x) = \prod_{m=1}^{M}\left(1 - \frac{\Gamma_u(N_g, x/(d_{3,m})^{-\epsilon_{\mathrm{L}}})}{\Gamma(N_g)}\right) = 1 + \Upsilon e^{-\tilde{\beta}x}x^{\tilde{l}}, \tag{14}$$

$$f_X(x) = \Upsilon\left[\tilde{l}e^{-\tilde{\beta}x}x^{\tilde{l}-1} - \tilde{\beta}e^{-\tilde{\beta}x}x^{\tilde{l}}\right] \tag{15}$$

where $\Gamma(\cdot)$ and $\Gamma_u(\cdot)$ respectively denote the complete gamma and upper incomplete gamma functions [37, Eqs. (8.310) and (8.350.2)]. In addition, $\tilde{\beta} \triangleq \sum_{t=1}^{m}(d_{3,q_t})^{\epsilon_{\mathrm{L}}}$, $\tilde{l} \triangleq \sum_{t=1}^{m}\ell_t$, and

$$\Upsilon \triangleq \sum_{m=1}^{M}(-1)^m \sum_{q_1=1}^{M-m+1}\cdots\sum_{q_m=q_{m-1}+1}^{M}\sum_{\ell_1=0}^{N_g-1}\cdots\sum_{\ell_m=0}^{N_g-1}\prod_{t=1}^{m}\left(\frac{(d_{3,q_t})^{\epsilon_{\mathrm{L}}}}{\ell_t!}\right). \tag{16}$$

Note that we assume the same number of multipath components for the expressions of (14) and (15), N_g, across the channels from M S-RRHs to the PRX. For non-identical number of multipath components, we can make them work by changing (16) as

$$\Upsilon \triangleq \sum_{m=1}^{M}(-1)^m \sum_{q_1=1}^{M-m+1}\cdots\sum_{q_m=q_{m-1}+1}^{M}\sum_{\ell_1=0}^{N_{g,q_1}-1}\cdots\sum_{\ell_m=0}^{N_{g,q_m}-1}\prod_{t=1}^{m}\left(\frac{(d_{3,q_t})^{\epsilon_{\mathrm{L}}}}{\ell_t!}\right) \tag{17}$$

where $N_{g,m} \triangleq \mathbb{L}(\tilde{\boldsymbol{g}}_{m,\mathrm{L}})$. Note that having updated equations (14)-(17), the distribution of the RV X can be used even for multiple PRXs. When the channels from M S-RRHs to the PRX also follow the model as that of the channel model either from the PTX to the SRX or from M S-RRHS to the SRX, then $F_X(x)$ should be replaced by $F_X(x) = \mathcal{G}F_{X,\mathrm{L}}(x) + (1-\mathcal{G})F_{X,\mathrm{nL}}(x)$ due to the employed binary Bernoulli process. Similarly, it is necessary to update $f_X(x)$ as follows: $f_X(x) = \mathcal{G}f_{X,\mathrm{L}}(x) + (1-\mathcal{G})f_{X,\mathrm{nL}}(x)$.

2) Distributions of the RVs A_{L} and A_{nL}: In the frequency selective fading, distributions of the RVs A_{L} and A_{nL} are given by

$$F_{A,\mathrm{L}}(x) = 1 - \sum_{k=0}^{N_{h,\mathrm{L}}-1}\frac{e^{-x/\alpha_{h,\mathrm{L}}}}{\Gamma(k+1)}(\alpha_{h,\mathrm{L}})^{-k}x^k \text{ and}$$

$$F_{A,\mathrm{nL}}(x) = 1 - \sum_{k=0}^{N_{h,\mathrm{nL}}-1}\frac{e^{-x/\alpha_{h,\mathrm{nL}}}}{\Gamma(k+1)}(\alpha_{h,\mathrm{nL}})^{-k}x^k \tag{18}$$

where $N_{h,\mathrm{L}} \triangleq \sum_{m=1}^{M}N_{h,\mathrm{L},m}$ and $N_{h,\mathrm{nL}} \triangleq \sum_{m=1}^{M}N_{h,\mathrm{nL},m}$.

3) Distribution of the interference power conditioned on a given distance d_2: Due to CP-SC transmissions, the conditional density of primary user's interference power received at the SRX at a given distance d_2, denoted by RV B, is given by

$$f_B(x|d_2) = \frac{\mathcal{G}x^{\hat{N}_{\mathrm{L}}-1}}{\Gamma(\hat{N}_{\mathrm{L}})(P_P(d_2)^{-\epsilon_{\mathrm{L}}})^{\hat{N}_{\mathrm{L}}}}e^{-\frac{x}{P_P(d_2)^{-\epsilon_{\mathrm{L}}}}} + \frac{(1-\mathcal{G})x^{\hat{N}_{\mathrm{nL}}-1}}{\Gamma(\hat{N}_{\mathrm{nL}})(P_P(d_2)^{-\epsilon_{\mathrm{nL}}})^{\hat{N}_{\mathrm{nL}}}}e^{-\frac{x}{P_P(d_2)^{-\epsilon_{\mathrm{nL}}}}} \tag{19}$$

where $\hat{N}_{\mathrm{L}} \triangleq QN_{f,\mathrm{L}}$ and $\hat{N}_{\mathrm{nL}} = QN_{f,\mathrm{nL}}$.

4) Distribution of the SA RV Y: Since the distribution of the SA Y is not available in existing literature, we provide its closed expression in Theorem 1.

Theorem 1: In the i.n.i.d. frequency selective fading channel, the distribution of the SA Y at a fixed location of the SRX is given by

$$\begin{aligned} F_{Y,\mathrm{SA}}(x) &= 1-\Bigg(\mathcal{G}\mathcal{F}\sum_{k=0}^{N_{h,\mathrm{L}}-1}\mathbb{B}_{\mathrm{L,L}}x^{-\hat{N}_{\mathrm{L}}}\mathbb{A}_{\mathrm{L,L}}+\mathcal{G}(1-\mathcal{F})\sum_{k=0}^{N_{h,\mathrm{L}}-1}\mathbb{B}_{\mathrm{L,nL}}x^{-\hat{N}_{\mathrm{nL}}}\mathbb{A}_{\mathrm{L,nL}}+\\ &\quad (1-\mathcal{G})\mathcal{F}\sum_{k=0}^{N_{h,\mathrm{nL}}-1}\mathbb{B}_{\mathrm{nL,L}}x^{-\hat{N}_{\mathrm{L}}}\mathbb{A}_{\mathrm{nL,L}}+(1-\mathcal{G})(1-\mathcal{F})\sum_{k=0}^{N_{h,\mathrm{nL}}-1}\mathbb{B}_{\mathrm{nL,nL}}x^{-\hat{N}_{\mathrm{nL}}}\mathbb{A}_{\mathrm{nL,nL}}\Bigg)\\ &= 1-J_A. \end{aligned} \tag{20}$$

In (20), we have defined the following terms:

$$\begin{aligned} \mathbb{A}_{\mathrm{L,L}} &\triangleq (R)^{\mu_{\mathrm{L}}\epsilon_{\mathrm{L}}}{}_2F_1\Big(\mu_{\mathrm{L}},k+\hat{N}_{\mathrm{L}};\mu_{\mathrm{L}}+1;-z_1^+\Big)-(R_{\min})^{\mu_{\mathrm{L}}\epsilon_{\mathrm{L}}}{}_2F_1\Big(\mu_{\mathrm{L}},k+\hat{N}_{\mathrm{L}};\mu_{\mathrm{L}}+1;-z_1^-\Big),\\ \mathbb{A}_{\mathrm{L,nL}} &\triangleq (R)^{\mu_{\mathrm{nL}}\epsilon_{\mathrm{nL}}}{}_2F_1\Big(\mu_{\mathrm{nL}},k+\hat{N}_{\mathrm{nL}};\mu_{\mathrm{nL}}+1;-z_2^+\Big)-(R_{\min})^{\mu_{\mathrm{nL}}\epsilon_{\mathrm{nL}}}{}_2F_1\Big(\mu_{\mathrm{nL}},k+\hat{N}_{\mathrm{nL}};\mu_{\mathrm{nL}}+1;-z_2^-\Big),\\ \mathbb{A}_{\mathrm{nL,L}} &\triangleq (R)^{\mu_{\mathrm{L}}\epsilon_{\mathrm{L}}}{}_2F_1\Big(\mu_{\mathrm{L}},k+\hat{N}_{\mathrm{L}};\mu_{\mathrm{L}}+1;-z_3^+\Big)-(R_{\min})^{\mu_{\mathrm{L}}\epsilon_{\mathrm{L}}}{}_2F_1\Big(\mu_{\mathrm{L}},k+\hat{N}_{\mathrm{L}};\mu_{\mathrm{L}}+1;-z_3^-\Big),\ \text{and}\\ \mathbb{A}_{\mathrm{nL,nL}} &\triangleq (R)^{\mu_{\mathrm{nL}}\epsilon_{\mathrm{nL}}}{}_2F_1\Big(\mu_{\mathrm{nL}},k+\hat{N}_{\mathrm{nL}};\mu_{\mathrm{nL}}+1;-z_4^+\Big)-(R_{\min})^{\mu_{\mathrm{nL}}\epsilon_{\mathrm{nL}}}{}_2F_1\Big(\mu_{\mathrm{nL}},k+\hat{N}_{\mathrm{nL}};\mu_{\mathrm{nL}}+1;-z_4^-\Big) \end{aligned} \tag{21}$$

with

$$\begin{aligned} \mathbb{B}_{\mathrm{L,L}} &\triangleq \frac{(\alpha_{h,\mathrm{L}})^{-\hat{N}_{\mathrm{L}}}}{\Gamma(k+1)}\frac{(P_p)^{\hat{N}_{\mathrm{L}}}\Gamma(k+\hat{N}_{\mathrm{L}})}{\Gamma(\hat{N}_{\mathrm{L}})}\frac{D_R}{\mu_{\mathrm{L}}\epsilon_{\mathrm{L}}},\ \mathbb{B}_{\mathrm{L,nL}} \triangleq \frac{(\alpha_{h,\mathrm{L}})^{-\hat{N}_{\mathrm{nL}}}}{\Gamma(k+1)}\frac{(P_p)^{\hat{N}_{\mathrm{nL}}}\Gamma(k+\hat{N}_{\mathrm{nL}})}{\Gamma(\hat{N}_{\mathrm{nL}})}\frac{D_R}{\mu_{\mathrm{nL}}\epsilon_{\mathrm{nL}}},\\ \mathbb{B}_{\mathrm{nL,L}} &\triangleq \frac{(\alpha_{h,\mathrm{nL}})^{-\hat{N}_{\mathrm{L}}}}{\Gamma(k+1)}\frac{(P_p)^{\hat{N}_{\mathrm{L}}}\Gamma(k+\hat{N}_{\mathrm{L}})}{\Gamma(\hat{N}_{\mathrm{L}})}\frac{D_R}{\mu_{\mathrm{L}}\epsilon_{\mathrm{L}}},\ \mathbb{B}_{\mathrm{nL,nL}} \triangleq \frac{(\alpha_{h,\mathrm{nL}})^{-\hat{N}_{\mathrm{nL}}}}{\Gamma(k+1)}\frac{(P_p)^{\hat{N}_{\mathrm{nL}}}\Gamma(k+\hat{N}_{\mathrm{nL}})}{\Gamma(\hat{N}_{\mathrm{nL}})}\frac{D_R}{\mu_{\mathrm{nL}}\epsilon_{\mathrm{nL}}},\\ \mu_{\mathrm{L}} &\triangleq 2/\epsilon_{\mathrm{L}}+\hat{N}_{\mathrm{L}},\mu_{\mathrm{nL}} \triangleq 2/\epsilon_{\mathrm{nL}}+\hat{N}_{\mathrm{nL}},\ \text{and}\ D_R \triangleq \frac{2}{(R^2-R_{\min}^2)}. \end{aligned}$$

In addition,

$$\begin{aligned} z_1^+ &\triangleq \frac{(R)^{\epsilon_{\mathrm{L}}}\alpha_{h,\mathrm{L}}}{P_px},\ z_1^- \triangleq \frac{(R_{\min})^{\epsilon_{\mathrm{L}}}\alpha_{h,\mathrm{L}}}{P_px},\ z_2^+ \triangleq \frac{(R)^{\epsilon_{\mathrm{nL}}}\alpha_{h,\mathrm{L}}}{P_px},\ z_2^- \triangleq \frac{(R_{\min})^{\epsilon_{\mathrm{nL}}}\alpha_{h,\mathrm{L}}}{P_px},\\ z_3^+ &\triangleq \frac{(R)^{\epsilon_{\mathrm{L}}}\alpha_{h,\mathrm{nL}}}{P_px},\ z_3^- \triangleq \frac{(R_{\min})^{\epsilon_{\mathrm{L}}}\alpha_{h,\mathrm{nL}}}{P_px},\ z_4^+ \triangleq \frac{(R)^{\epsilon_{\mathrm{nL}}}\alpha_{h,\mathrm{nL}}}{P_px},\ \text{and}\ z_4^- \triangleq \frac{(R_{\min})^{\epsilon_{\mathrm{nL}}}\alpha_{h,\mathrm{nL}}}{P_px}. \end{aligned}$$

The Gauss hypergeometric function [37, Eq. (9.100)] is denoted by ${}_2F_1(\cdot,\cdot;\cdot;\cdot)$. Note that since J_A can be derived easily from (20), we do not provide its detailed expression.

Proof: See Appendix A. ■

We can compute J_1 from (14) and (20) as follows:

$$J_1 = F_{Y,\mathrm{SA}}(x/P_T)F_X(\mu). \tag{22}$$

Thus, we do not provide its detailed expression. Although a closed-form expression for J_1 is obtained, a more challenging task, the computation of J_2 in (13), is left.

Corollary 1: According to [38, Eqs. (07.23.06.0021.01) and (07.23.06.0002.01)] and depending on the absolute value of z, with $|z| \neq 1$ and $|a-b| \notin \mathbb{N}_0$, we represent ${}_2F_1(a,b;c;z)$ as follows:

$$
{}_2F_1(a,b;c;z) = \begin{cases} \sum_{k=0}^{\infty} \frac{(a)_{[k]}(b)_{[k]}(z)^k}{(c)_{[k]}}, |z|<1, \\ \frac{\Gamma(b-a)\Gamma(c)(-z)^{-a}}{\Gamma(b)\Gamma(c-a)} \sum_{k=0}^{\infty} \frac{(a)_{[k]}(a-c+1)_{[k]}(z)^{-k}}{\Gamma(k+1)(a-b+1)_{[k]}} + \\ \quad \frac{\Gamma(a-b)\Gamma(c)(-z)^{-b}}{\Gamma(a)\Gamma(c-b)} \sum_{k=0}^{\infty} \frac{(b)_{[k]}(b-c+1)_{[k]}(z)^{-k}}{\Gamma(k+1)(-a+b+1)_{[k]}}, |z|>1, \end{cases} \tag{23}
$$

where $(a)_{[k]} \triangleq \frac{\Gamma(a+k)}{\Gamma(a)}$.

Note that the absolute difference of the first two parameters of Gauss hypergeometric functions used in (20) are not positive integers, so that *Corollary* 1 will be used in the following analysis.

Corollary 2: According to *Corollary* 1, (20) can be expressed as follows:

$$
\begin{aligned}
F_{Y,\mathrm{SA}}(x) = 1 - \Bigg(& \mathcal{G}\mathcal{F} \sum_{k=0}^{N_{h,\mathrm{L}}-1} \mathbb{B}_{\mathrm{L,L}} \Bigg(\left\langle \begin{array}{c} A_{\mathrm{L,L},11} x^{-(i_k+\hat{N}_{\mathrm{L}})}, \ |-z_1^+|<1 \\ A_{\mathrm{L,L},12} x^{2/\epsilon_{\mathrm{L}}} + A_{\mathrm{L,L},13} x^{-(i_k+k)}, \ |-z_1^+|>1 \end{array} \right\rangle - \\
& \left\langle \begin{array}{c} A_{\mathrm{L,L},21} x^{-(i_k+\hat{N}_{\mathrm{L}})}, \ |-z_1^-|<1 \\ A_{\mathrm{L,L},22} x^{2/\epsilon_{\mathrm{L}}} + A_{\mathrm{L,L},23} x^{-(i_k+k)}, \ |-z_1^-|>1 \end{array} \right\rangle \Bigg) + \\
& \mathcal{G}(1-\mathcal{F}) \sum_{k=0}^{N_{h,\mathrm{L}}-1} \mathbb{B}_{\mathrm{L,nL}} \Bigg(\left\langle \begin{array}{c} A_{\mathrm{L,nL},11} x^{-(i_k+\hat{N}_{\mathrm{nL}})}, \ |-z_2^+|<1 \\ A_{\mathrm{L,nL},12} x^{2/\epsilon_{\mathrm{nL}}} + A_{\mathrm{nL},13} x^{-(i_k+k)}, \ |-z_2^+|>1 \end{array} \right\rangle - \\
& \left\langle \begin{array}{c} A_{\mathrm{L,nL},21} x^{-(i_k+\hat{N}_{\mathrm{nL}})}, \ |-z_2^-|<1 \\ A_{\mathrm{L,nL},22} x^{2/\epsilon_{\mathrm{nL}}} + A_{\mathrm{L,nL},23} x^{-(i_k+k)}, \ |-z_2^-|>1 \end{array} \right\rangle \Bigg) + \\
& (1-\mathcal{G})\mathcal{F} \sum_{k=0}^{N_{h,\mathrm{nL}}-1} \mathbb{B}_{\mathrm{nL,L}} \Bigg(\left\langle \begin{array}{c} A_{\mathrm{nL,L},11} x^{-(i_k+\hat{N}_{\mathrm{L}})}, \ |-z_3^+|<1 \\ A_{\mathrm{nL,L},12} x^{2/\epsilon_{\mathrm{L}}} + A_{\mathrm{nL,L},13} x^{-(i_k+k)}, \ |-z_3^+|>1 \end{array} \right\rangle - \\
& \left\langle \begin{array}{c} A_{\mathrm{nL,L},21} x^{-(i_k+\hat{N}_{\mathrm{L}})}, \ |-z_3^-|<1 \\ A_{\mathrm{nL,L},22} x^{2/\epsilon_{\mathrm{L}}} + A_{\mathrm{nL,L},23} x^{-(i_k+k)}, \ |-z_3^-|>1 \end{array} \right\rangle \Bigg) + \\
& (1-\mathcal{G})(1-\mathcal{F}) \sum_{k=0}^{N_{h,\mathrm{nL}}-1} \mathbb{B}_{\mathrm{nL,nL}} \Bigg(\left\langle \begin{array}{c} A_{\mathrm{nL,nL},11} x^{-(i_k+\hat{N}_{\mathrm{nL}})}, \ |-z_4^+|<1 \\ A_{\mathrm{nL,nL},12} x^{2/\epsilon_{\mathrm{nL}}} + A_{\mathrm{nL,nL},13} x^{-(i_k+k)}, \ |-z_4^+|>1 \end{array} \right\rangle - \\
& \left\langle \begin{array}{c} A_{\mathrm{nL,nL},21} x^{-(i_k+\hat{N}_{\mathrm{nL}})}, \ |-z_4^-|<1 \\ A_{\mathrm{nL,nL},22} x^{2/\epsilon_{\mathrm{nL}}} + A_{\mathrm{nL,nL},23} x^{-(i_k+k)}, \ |-z_4^-|>1 \end{array} \right\rangle \Bigg) \Bigg)
\end{aligned} \tag{24}
$$

where $\left\langle \begin{array}{cc} \ddots, & c_1 \\ \ddots, & c_2 \end{array} \right\rangle$ denotes a conditional equation depending on two conditions c_1 and c_2, and three key equations are defined as follows:

$$
\begin{aligned}
A_{\mathrm{L,L},11} &= (R)^{2+\epsilon_{\mathrm{L}}\hat{N}_{\mathrm{L}}} \left(\frac{P_p}{\alpha_{h,\mathrm{L}}} \right)^{-k-\hat{N}_{\mathrm{L}}} \sum_{ik=0}^{N} \frac{(2/\epsilon_{\mathrm{L}}+\hat{N}_{\mathrm{L}})_{[i_k]}(k+\hat{N}_{\mathrm{L}})_{[i_k]}}{\Gamma(i_k+1)(2/\epsilon_{\mathrm{L}}+\hat{N}_{\mathrm{L}}+1)_{[i_k]}} (C_1)^{i_k}, \\
A_{\mathrm{L,L},12} &= \left(\frac{P_p}{\alpha_{h,\mathrm{L}}} \right)^{2/\epsilon_{\mathrm{L}}-k} C_2 \Gamma(2/\epsilon_{\mathrm{L}}+\hat{N}_{\mathrm{L}}+1), \text{ and}
\end{aligned}
$$

$$A_{\mathrm{L,L,13}} = \frac{2/\epsilon_{\mathrm{L}}+\hat{N}_{\mathrm{L}}}{2/\epsilon_{\mathrm{L}}-k}R^{2-k\epsilon_{\mathrm{L}}}\sum_{i_k=0}^{N}\frac{(k+\hat{N}_{\mathrm{L}})_{[i_k]}(k-2/\epsilon_{\mathrm{L}})_{[i_k]}}{\Gamma(i_k+1)(k-2/\epsilon_{\mathrm{L}}+1)_{[i_k]}}(C_1)^{-i_k} \tag{25}$$

where $C_1 \triangleq -\frac{(R)^{\epsilon_{\mathrm{L}}}\alpha_{h,\mathrm{L}}}{P_p}$ and $C_2 \triangleq \frac{\Gamma(k-2/\epsilon_{\mathrm{L}})}{\Gamma(k+\hat{N}_{\mathrm{L}})}$. Based on (25), additional terms can be computed as follows:

$$\begin{aligned}
A_{\mathrm{L,L,2}i} &= A_{\mathrm{L,L,1}i}\Big|_{R\to R_{\min}},\ A_{\mathrm{L,nL,1}i} = A_{\mathrm{L,L,1}i}\Big|_{\epsilon_{\mathrm{L}}\to\epsilon_{\mathrm{nL}},\mu_{\mathrm{L}}\to\mu_{\mathrm{nL}},\hat{N}_{\mathrm{L}}\to\hat{N}_{\mathrm{nL}}},\\
A_{\mathrm{L,nL,2}i} &= A_{\mathrm{L,nL,1}i}\Big|_{R\to R_{\min}},\ A_{\mathrm{nL,L,1}i} = A_{\mathrm{L,L,1}i}\Big|_{\alpha_{h,\mathrm{L}}\to\alpha_{h,\mathrm{nL}}},\\
A_{\mathrm{nL,nL,1}i} &= A_{\mathrm{L,L,1}i}\Big|_{\alpha_{h,\mathrm{L}}\to\alpha_{h,\mathrm{nL}},\epsilon_{\mathrm{L}}\to\epsilon_{\mathrm{nL}},\mu_{\mathrm{L}}\to\mu_{\mathrm{nL}},\hat{N}_{\mathrm{L}}\to\hat{N}_{\mathrm{nL}}}, \text{and}\\
A_{\mathrm{nL,L,2}i} &= A_{\mathrm{nL,L,1}i}\Big|_{R\to R_{\min}},\ \text{for } i=1,2,\ \text{and } 3.
\end{aligned} \tag{26}$$

Note that *Corollary* 2 provides that $F_{Y,\mathrm{SA}}(x)$ can be expressed by a finite sum of Hypergeometric series.

Corollary 3: The closed-form expression for J_2 can be derived as

$$\begin{aligned}
J_2(x) = (1-F_X(\mu)) - \Bigg(&\mathcal{GF}\sum_{k=0}^{N_{h,\mathrm{L}}-1}\mathbb{B}_{\mathrm{L,L}}\Bigg(\Bigg\langle \begin{matrix} C_{\mathrm{L,L,11}}(\frac{x}{I_p})^{-(i_k+\hat{N}_{\mathrm{L}})},\ |-z_1^+|<1 \\ C_{\mathrm{L,L,12}}(\frac{x}{I_p})^{2/\epsilon_{\mathrm{L}}}+C_{\mathrm{L,L,13}}(\frac{x}{I_p})^{-(i_k+k)},\ |-z_1^+|>1 \end{matrix}\Bigg\rangle -\\
&\Bigg\langle \begin{matrix} C_{\mathrm{L,L,21}}(\frac{x}{I_p})^{-(i_k+\hat{N}_{\mathrm{L}})},\ \text{for } |-z_1^-|<1 \\ C_{\mathrm{L,L,22}}(\frac{x}{I_p})^{2/\epsilon_{\mathrm{L}}}+C_{\mathrm{L,L,23}}(\frac{x}{I_p})^{-(i_k+k)},\ \text{for } |-z_1^-|>1 \end{matrix}\Bigg\rangle\Bigg)+\\
&\mathcal{G}(1-\mathcal{F})\sum_{k=0}^{N_{h,\mathrm{L}}-1}\mathbb{B}_{\mathrm{L,nL}}\Bigg(\Bigg\langle \begin{matrix} C_{\mathrm{L,nL,11}}(\frac{x}{I_p})^{-(i_k+\hat{N}_{\mathrm{nL}})},\ \text{for } |-z_2^+|<1 \\ C_{\mathrm{L,nL,12}}(\frac{x}{I_p})^{2/\epsilon_{\mathrm{nL}}}+C_{\mathrm{nL,13}}(\frac{x}{I_p})^{-(i_k+k)},\ \text{for } |-z_2^+|>1 \end{matrix}\Bigg\rangle -\\
&\Bigg\langle \begin{matrix} C_{\mathrm{L,nL,21}}(\frac{x}{I_p})^{-(i_k+\hat{N}_{\mathrm{nL}})},\ \text{for } |-z_2^-|<1 \\ C_{\mathrm{L,nL,22}}(\frac{x}{I_p})^{2/\epsilon_{\mathrm{nL}}}+C_{\mathrm{L,nL,23}}(\frac{x}{I_p})^{-(i_k+k)},\ \text{for } |-z_2^-|>1 \end{matrix}\Bigg\rangle\Bigg)+\\
&(1-\mathcal{G})\mathcal{F}\sum_{k=0}^{N_{h,\mathrm{nL}}-1}\mathbb{B}_{\mathrm{nL,L}}\Bigg(\Bigg\langle \begin{matrix} C_{\mathrm{nL,L,11}}(\frac{x}{I_p})^{-(i_k+\hat{N}_{\mathrm{L}})},\ \text{for } |-z_3^+|<1 \\ C_{\mathrm{nL,L,12}}(\frac{x}{I_p})^{2/\epsilon_{\mathrm{L}}}+C_{\mathrm{nL,L,13}}(\frac{x}{I_p})^{-(i_k+k)},\ \text{for } |-z_3^+|>1 \end{matrix}\Bigg\rangle -\\
&\Bigg\langle \begin{matrix} C_{\mathrm{nL,L,21}}(\frac{x}{I_p})^{-(i_k+\hat{N}_{\mathrm{L}})},\ \text{for } |-z_3^-|<1 \\ C_{\mathrm{nL,L,22}}(\frac{x}{I_p})^{2/\epsilon_{\mathrm{L}}}+C_{\mathrm{nL,L,23}}(\frac{x}{I_p})^{-(i_k+k)},\ \text{for } |-z_3^-|>1 \end{matrix}\Bigg\rangle\Bigg)+\\
&(1-\mathcal{G})(1-\mathcal{F})\sum_{k=0}^{N_{h,\mathrm{nL}}-1}\mathbb{B}_{\mathrm{nL,nL}}\Bigg(\Bigg\langle \begin{matrix} C_{\mathrm{nL,nL,11}}(\frac{x}{I_p})^{-(i_k+\hat{N}_{\mathrm{nL}})},\ \text{for } |-z_4^+|<1 \\ C_{\mathrm{nL,nL,12}}(\frac{x}{I_p})^{2/\epsilon_{\mathrm{nL}}}+C_{\mathrm{nL,nL,13}}(\frac{x}{I_p})^{-(i_k+k)},\ \text{for } |-z_4^+|>1 \end{matrix}\Bigg\rangle -\\
&\Bigg\langle \begin{matrix} C_{\mathrm{nL,nL,21}}(\frac{x}{I_p})^{-(i_k+\hat{N}_{\mathrm{nL}})},\ \text{for } |-z_4^-|<1 \\ C_{\mathrm{nL,nL,22}}(\frac{x}{I_p})^{2/\epsilon_{\mathrm{nL}}}+C_{\mathrm{nL,nL,23}}x^{-(i_k+k)},\ \text{for } |-z_4^-|>1 \end{matrix}\Bigg\rangle\Bigg)\Bigg)\\
= 1-F_X(\mu)+J_B.&
\end{aligned} \tag{27}$$

In (27), we have defined $C_{\mathrm{L,L,11}} = A_{\mathrm{L,L,11}}\Upsilon\Big[\tilde{l}(\tilde{\beta})^{-(\tilde{l}-(i_k+\hat{N}_{\mathrm{L}}))}\Gamma_u(\tilde{l}-(i_k+\hat{N}_{\mathrm{L}}),\mu\tilde{\beta})-\tilde{\beta}(\tilde{\beta})^{-(\tilde{l}-(i_k+\hat{N}_{\mathrm{L}})+1)}\Gamma_u(\tilde{l}-(i_k+\hat{N}_{\mathrm{L}})+1,\mu\tilde{\beta})\Big]$, $C_{\mathrm{L,L,12}} = A_{\mathrm{L,L,12}}\Upsilon\Big[\tilde{l}(\tilde{\beta})^{-(\tilde{l}+2/\epsilon_{\mathrm{L}})}\Gamma_u(\tilde{l}+2/\epsilon_{\mathrm{L}},\mu\tilde{\beta})-\tilde{\beta}(\tilde{\beta})^{-(\tilde{l}+2/\epsilon_{\mathrm{L}}+1)}\Gamma_u(\tilde{l}+2/\epsilon_{\mathrm{L}}+1,\mu\tilde{\beta})\Big]$, and $C_{\mathrm{L,L,13}} = A_{\mathrm{L,L,13}}\Upsilon\Big[\tilde{l}(\tilde{\beta})^{-(\tilde{l}-(i_k+k))}\Gamma_u(\tilde{l}-(i_k+k),\mu\tilde{\beta})-\tilde{\beta}(\tilde{\beta})^{-(\tilde{l}-(i_k+k)+1)}\Gamma_u(\tilde{l}-(i_k+k)+1,\mu\tilde{\beta})\Big]$. Based on these three key definitions, we can readily derive the other remaining terms as in the computations provided in (26), so that we do not provide their corresponding expressions. Without detailed description, J_B can be easily derived from (27).

B. Outage Probability Analysis

Theorem 2: Based on *Theorem* 1 and *Corollary* 3, the desired $F_{\gamma_{\text{SIR}}}(x)$ can be derived as follows:

$$F_{\gamma_{\text{SIR}}}(x) = 1 - J_A\Big|_{x\to\frac{x}{P_T}} F_X(\mu) + J_B \tag{28}$$

where J_A and J_B are respectively defined in *Theorem* 1 and *Corollary* 3.

With an available $F_{\gamma_{\text{SIR}}}(x)$. The outage probability at a given SIR threshold x_{th} is given by

$$P_{\text{outage}}(x_{\text{th}}) = 1 - J_A\Big|_{x\to\frac{x_{\text{th}}}{P_T}} F_X(\mu) + J_B|_{x\to x_{\text{th}}}. \tag{29}$$

When $\mu = \frac{I_p}{P_T}$ is not a constant, two distinctive operating regions can be specified.

1) The region with $\mu << 1$ or a constant I_p : In this region, $F_X(\mu) \approx 0$, so that we can have the following approximate expression for the outage probability

$$P^{\mu<<1}_{\text{outage}}(x_{\text{th}}) \approx 1 + J_B|_{x\to x_{\text{th}}} \tag{30}$$

which is provided in the following Corollary.

Corollary 4: In the region of $\mu << 1$, when I_p is constant, the outage probability is limited by

$$P^{\mu<<1}_{\text{outage}}(x_{\text{th}}) = 1 - F_X(\mu) - \Bigg(\mathcal{GF}\Big(\frac{x_{\text{th}}}{I_p}\Big)^{-\hat{N}_{\text{L}}}\sum_{k=0}^{N_{h,\text{L}}-1}\mathbb{B}_{\text{L,L}}\mathbb{D}_{\text{L,L}} + \mathcal{G}(1-\mathcal{F})\Big(\frac{x_{\text{th}}}{I_p}\Big)^{-\hat{N}_{\text{nL}}}\sum_{k=0}^{N_{h,\text{L}}-1}\mathbb{B}_{\text{L,nL}}\mathbb{D}_{\text{L,nL}} +$$
$$(1-\mathcal{G})\mathcal{F}\Big(\frac{x_{\text{th}}}{I_p}\Big)^{-\hat{N}_{\text{L}}}\sum_{k=0}^{N_{h,\text{nL}}-1}\mathbb{B}_{\text{nL,L}}\mathbb{D}_{\text{nL,L}} + (1-\mathcal{G})(1-\mathcal{F})\Big(\frac{x_{\text{th}}}{I_p}\Big)^{-\hat{N}_{\text{nL}}}\sum_{k=0}^{N_{h,\text{nL}}-1}\mathbb{B}_{\text{nL,nL}}\mathbb{D}_{\text{nL,nL}}\Bigg) \tag{31}$$

where $\mathbb{D}_{\text{L,L}}$, $\mathbb{D}_{\text{L,nL}}$, $\mathbb{D}_{\text{nL,L}}$, and $\mathbb{D}_{\text{nL,nL}}$ are defined in Appendix B with their derivations.

Note that *Corollary 4* verifies that $P^{\mu<<1}_{\text{outage}}(x_{\text{th}})$ is proportional to either $\left(\frac{x_{\text{th}}}{I_p}\right)^{-\hat{N}_{\text{L}}}$ or $\left(\frac{x_{\text{th}}}{I_p}\right)^{-\hat{N}_{\text{nL}}}$. Thus, when I_p is constant, $P^{\mu<<1}_{\text{outage}}(x_{\text{th}})$ becomes constant independent of I_p.

2) The region with $\mu > 1$ or a constant μ: In this region, we can have the following

$$P^{\mu>1}_{\text{outage}}(x_{\text{th}}) \approx 1 - J_A\Big|_{x\to\frac{x_{\text{th}}}{P_T}} F_X(\mu) \approx 1 - J_A\Big|_{x\to\frac{x_{\text{th}}}{P_T}} \tag{32}$$

which can be derived from *Theorem 1*. Note that in this region, I_p has no impact on the outage probability, so that the considered system is out of the spectrum sharing region as P_T increases.

IV. Simulations

The following simulation setup is considered:

- As one example, we consider $B = 32$ and $N_{CP} = 8$, so that $K = 4$ is the maximum number of S-RRHs in the secondary users' network for dCDD. Without loss of generality, the proposed analysis can support any size of B and N_{CP}.
- Quadrature phase-shift keying (QPSK) modulation is used.
- According to [27], different path-loss exponents, such as $\epsilon_{\text{L}} = 2.09$ and $\epsilon_{\text{nL}} = 3.75$, are used. We assume $R_{\min} = 1$.
- The SRX is placed at the center of a circular shaped secondary users' communication cell of radius R, within which the PRX is placed at $(x_{\text{PRX}} = 0.2R, y_{\text{PRX}} = 0.2R)$.

- Four S-RRHs are respectively placed at random as follows: $R^{j(-0.0428)\pi}$, $R^{j(1.3707)\pi}$, $R^{j(0.4041)\pi}$, and $R^{j(-0.9967)\pi}$. When two S-RRHs are under servicing, we choose the first two S-RRHs.
- A fixed transmission power is assigned at all the PTXs as $P_P = 3$ dB.
- A fixed μ with $\mu = 1$ is used for all the simulations, which will be relaxed with a non-constant value in one simulation scenario.
- In specifying the upper limit of k in (23), 300 Hypergeometric series are selected from the empirical observations.
- In the simulations, a system serviced with a single S-RRH, i.e., $M = 1$, is recognized as the conventional system [20], [21], which does not use the dCDD scheme.
- We use the MATLAB for the link level simulations. At least 1,000,000 runs are used to obtain a very reliable empirical outage probability.

The curves obtained via link-level simulations are denoted by **Ex**. Analytical performance curves is denoted by **An**. The SIR threshold causing an outage is fixed at $x_{\rm th} = 1$ dB.

A. Verification of the outage probability

To verify the derivation of the outage probability, $P_{\text{outage}}(x_{\rm th})$, provided in *Theorem* 2, we used the following fixed system and channel parameters: ($N_g = 2$, $N_{f,\rm L} = 2$, $N_{f,\rm nL} = 3$) and ($\mathcal{G} = 0.8$ and $\mathcal{F} = 0.2$). The value of

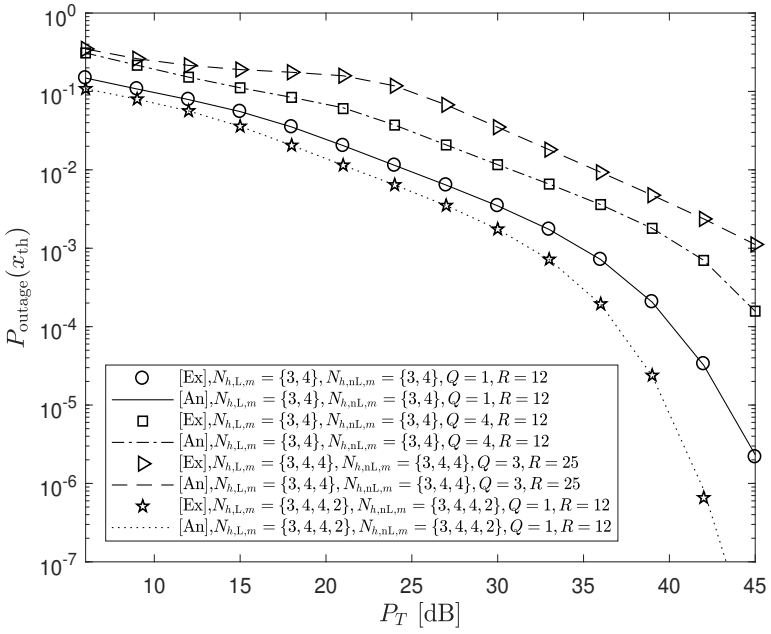

Fig. 2. $P_{\text{outage}}(x_{\rm th})$ for various values of M, Q, and R.

M, the number of S-RRHs in the simulation can be determined by the number of elements of $N_{h,\rm L,m}$ and $N_{h,\rm nL,m}$.

For example, from $N_{h,\mathrm{L},m} = \{3, 4\}$, two S-RRHs are in the system, whereas from $N_{h,\mathrm{L},m} = \{3, 4, 4, 2\}$, we can see that four S-RRHs are in the system.

In Fig. 2, we first compare the exact outage probability with its analytically derived outage probability, which was developed by *Theorem* 2 for various values of M, Q, and R. We can see the following facts:

- As Q increases, a higher outage probability can be observed due to more aggregated interference from Q PTXs.
- As M increases, a lower outage probability can be observed due to an increased desired signal power at the SRX in the secondary user's network.
- As either $N_{h,\mathrm{L}}$ or $N_{h,\mathrm{nL}}$ increases, a lower outage probability can be observed due to an increased desired signal power received from M S-RRHs.
- For the considered scenarios, we can see the accuracy of the analytically derived outage probability comparing with its corresponding exact one. Thus, we will mix them in the following outage probability analysis.

B. Impact of $N_{h,\mathrm{L},m}$ and $N_{h,\mathrm{nL},m}$ on the outage probability

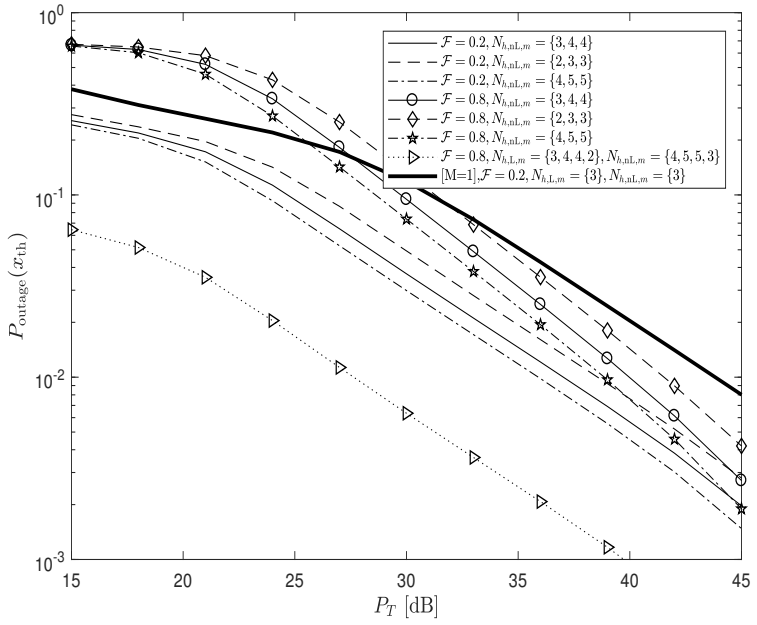

Fig. 3. Impact of $\mathcal{G}$ and $N_{h,\mathrm{nL},m}$ on the outage probability for various values of $\mathcal{G}$ and $\mathcal{F}$.

In the simulation of Fig. 3, we assume three S-RRHs in the system. For a fixed $N_{h,L,m} = \{3, 4, 4\}$, we investigate the different multipath components over nLoS path for two different values of $\mathcal{F}$. We use the following fixed system and channel parameters: ($Q = 2$, $N_g = 2$, $N_{f,\mathrm{L}} = 2$, $N_{f,\mathrm{nL}} = 3$, $\mathcal{G} = 0.8$, $R = 25$). From this figure, we can see that as $N_{h,\mathrm{nL}}$ is increased, a lower outage probability can be achieved. As an additional comparison, we also consider a fully populated spectrum sharing system with four S-RRHs. For $N_{h,\mathrm{L},m} = \{3, 4, 4, 2\}$ and $N_{h,\mathrm{L},m} = \{4, 5, 5, 3\}$,

a significant performance improvement on the outage probability can be observed. Since the maximum number of S-RRHs is determined by the block size of the transmission symbol, a larger value of B results in an improved outage probability when the maximum number of multipath components over the secondary user' network is same, and the secondary users' network can be fully populated by S-RRHs. This figure also shows that dCDD makes the considered system reduce the outage comparing with the system which uses only one S-RRH [20], [21].

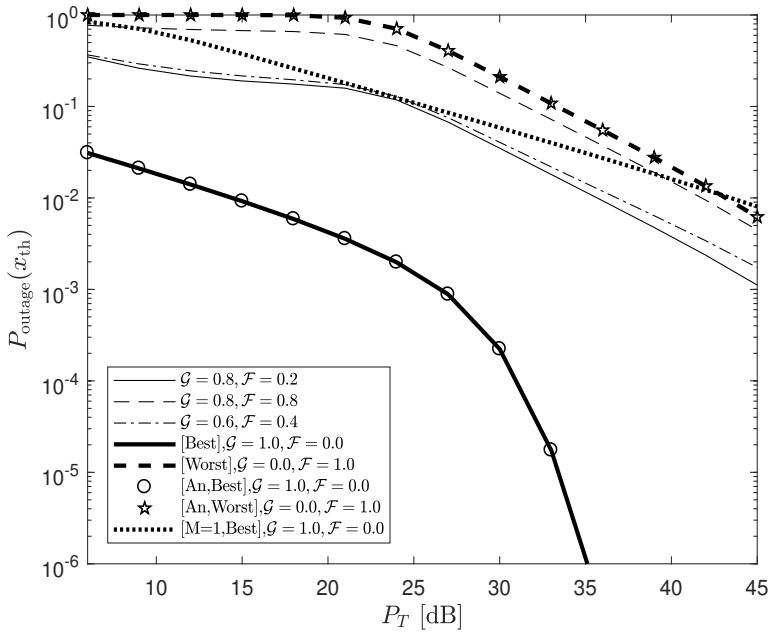

Fig. 4. Impact of $N_{h,\mathrm{L}}$, and $N_{h,\mathrm{nL}}$ on the outage probability for various values of $\mathcal{G}$ and $\mathcal{F}$.

In Fig. 4, we investigate another aspect of the impact of different number of multipath components in the secondary users' network on the outage probability for various values of $\mathcal{G}$ and $\mathcal{F}$. We use the following fixed parameters for this scenario as $(Q = 3, N_{h,\mathrm{L},m} = \{3,4,4\}, N_{h,\mathrm{nL},m} = \{3,4,4\}, R = 25, N_{f,\mathrm{L}} = 2, N_{f,\mathrm{nL}} = 3, N_g = 2)$. We also plot the best and worst outage probabilities in this scenario. The best outage probability can be obtained with LoS path between three S-RRHs and SRX and nLoS path between three PTXs and the SRX, that is, $\mathcal{G} = 1$ and $\mathcal{F} = 0$, whereas the worst outage probability can be obtained with nLoS path between three S-RRHs and the SRX, and LoS path between three PTXs and the SRX, that is, $\mathcal{G} = 0$ and $\mathcal{F} = 1$. For various values of $\mathcal{G}$ and $\mathcal{F}$, outage probabilities are placed between these two extreme outage probabilities. Especially, a significant gap exists between the best outage probability and others corresponding to the remaining scenarios. This figure also shows that the closed-form expression for the outage probability provides very accurate results even for two extreme outage probabilities. This figure also shows that dCDD makes the considered system achieve a significantly lower outage probability comparing with the system which uses only one S-RRH [20], [21].

In the following scenarios, we assume that the LoS and nLoS paths in the secondary users' network have the same number of multipath components. Thus, we will specify only the number of mulpath components of the LoS

path.

C. Impact of $\mathcal{F}$ on the outage probability

Since $\mathcal{F}$ models the random selection of interfering LoS and nLoS paths, this subsection investigate a different type of interference mixture in terms of $\mathcal{F}$. For various scenarios, we verify the impact of $\mathcal{F}$ on the outage probability at a fixed value of $P_T = \ 18$ dB. In addition, we used the following fixed system and channel parameters: $(N_{h,\mathrm{L},m} = \{3, 4, 4\}, N_g = 2, \mathcal{G} = 0.2, R = 25)$.

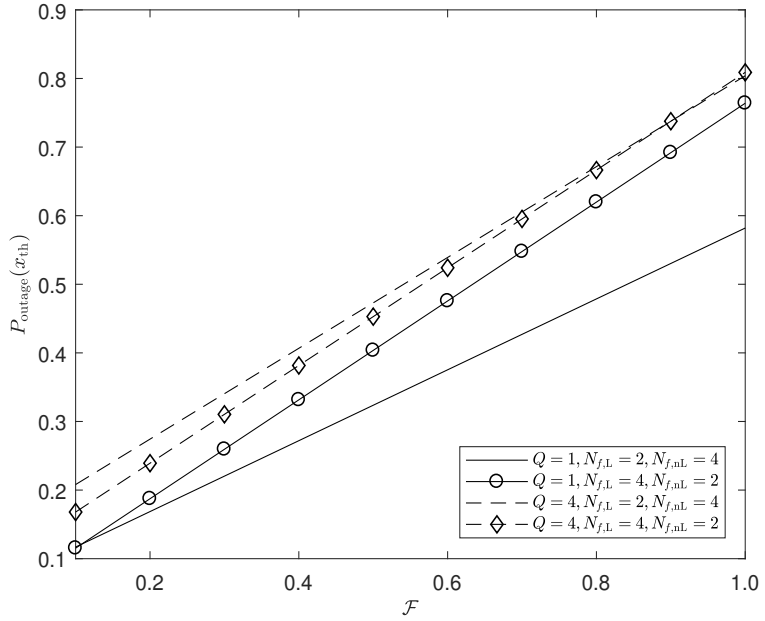

Fig. 5. Impact of $\mathcal{F}$ on the outage probability for various values of Q, $N_{f,\mathrm{L}}$, and $N_{f,\mathrm{nL}}$.

This figure shows the following facts:

- If we compare $(N_{f,\mathrm{L}} = 2, N_{f,\mathrm{nL}} = 4, Q = 1)$ with $(N_{f,\mathrm{L}} = 2, N_{f,\mathrm{nL}} = 4, Q = 4)$, the gap in the outage probability increases as $\mathcal{F}$ increases due a different path loss exponent over LoS and nLoS paths. However, when $Q = 4$, the gap caused by a different number of interfering multipath components is not so big as that of $Q = 1$ since interference is already enough to cause the outage.

D. Impact of $\mathcal{G}$ on the outage probability

Since $\mathcal{G}$ models the random selection of LoS and nLoS paths over the secondary users' network, this subsection investigate different type of a composite received signal in terms of $\mathcal{G}$. In generating Fig. 6, we used $M = 4$ with fixed values of $(N_{h,\mathrm{L},m} = \{3, 4, 4, 2\}, N_g = 2, P_T = \ 18$ dB). From this figure, we can see the following facts:

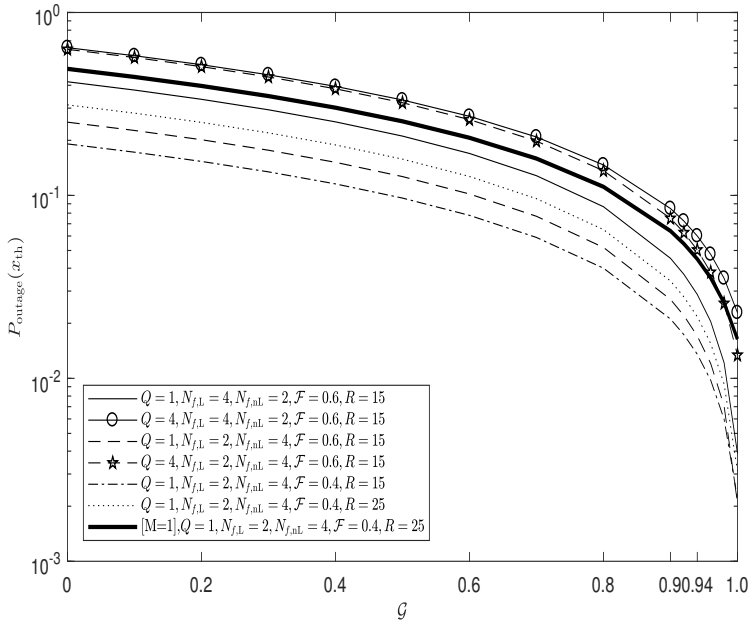

Fig. 6. Impact of $\mathcal{G}$ on the outage probability for various values of Q, $\mathcal{F}$, R, $N_{f,\text{L}}$ and $N_{f,\text{nL}}$.

- As $\mathcal{G}$ increases, the LoS path dominates, so that a better outage probability is achieved. Especially, as $\mathcal{G} \to 1$, the outage probability changes significantly. This scenario corresponds to the case, in which only the LoS path exists in the secondary users' network.
- Even a system which uses only one S-RRH, a similar behavior in the outage probability can be observed as $\mathcal{G} \to 1$. However, an intrinsic gap exists with respect to the dCDD based system.
- As R increases, a worse outage probability is achieved since the receive signal power at the SRX is reduced, in which the path loss exponent is the key parameter causing this result.

E. Impact of R on the outage probability

Since the size of the communication cell of the secondary users' network with respect to the SRX is also the key parameter in the system design, we investigate its impact on the outage probability. In this scenario, we use $M = 4$ with fixed values of $(N_{h,\text{L},m} = \{3, 4, 4, 2\}, N_g = 2, \mathcal{G} = 0.2, \mathcal{F} = 0.3$, and $P_T = \ 18$ dB), that is, the system is fully populated by four S-RRHs. From Fig. 7, we can observe the following facts:

- As R increases, a worse outage probability is obtained since R impacts more on the receive signal power than interference power at the SRX.
- At a fixed value of R, a more PTXs result in a worse outage probability as in previous several scenarios.
- Comparing $(N_{f,\text{L}} = 2, N_{f,\text{nL}} = 4)$ with $(N_{f,\text{L}} = 4, N_{f,\text{nL}} = 2)$, a more fluctuation can be observed with $(N_{f,\text{L}} = 2, N_{f,\text{nL}} = 4)$ due to a bigger change in the receive interference power at the SRX in the considered simulation set up. When $(N_{f,\text{L}} = 4, N_{f,\text{nL}} = 2)$, the outage probability does not change a lot in terms of

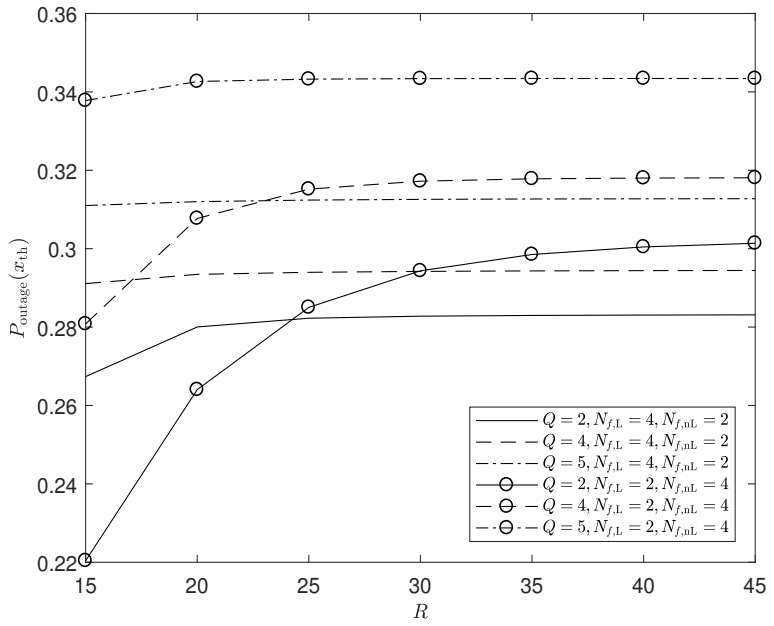

Fig. 7. Impact of R on the outage probability for various values of Q, $N_{f,\text{L}}$, and $N_{f,\text{nL}}$.

R since the multipath over the LoS path dominates and the LoS path has a less degradation in terms of the distance.

In the previous simulation scenarios, we assume that μ is constant. However, in the following subsection, we will investigate the impact of μ on the outage probability.

F. Impact of μ on the outage probability

In this scenario, we used $M = 4$ with fixed values of $(N_{h,\text{L},m} = \{3, 4, 4\}, N_g = 2, \mathcal{G} = 0.8, \mathcal{F} = 0.6)$. From Fig. 8, we can find the following facts:

- Two distinctive regions can separated as $\mu << 1$ and $\mu > 1$. In the region of $\mu << 1$, $J_B|_{x \to x_{\text{th}}}$ dominates the outage probability. Thus, we can see an outage probability floor, which is denoted by $P_{\text{outage}}^{\mu<<1}(x_{\text{th}})$. A similar observation was investigated by [21]. However, in the region of $\mu > 1$, $J_A|_{x \to \frac{x_{\text{th}}}{P_T}} F_X(\mu)$ dominates the outage probability. Thus, the outage probability is decreased inversely proportional to μ.
- A more number of S-RRHs in the secondary users' network impacts more on the outage probability in the region of $\mu > 1$ than that of the region of $\mu << 1$.
- The outage probability floor depends on the number of PTXs, that is, interference from PTXs impacts the outage probability floor.

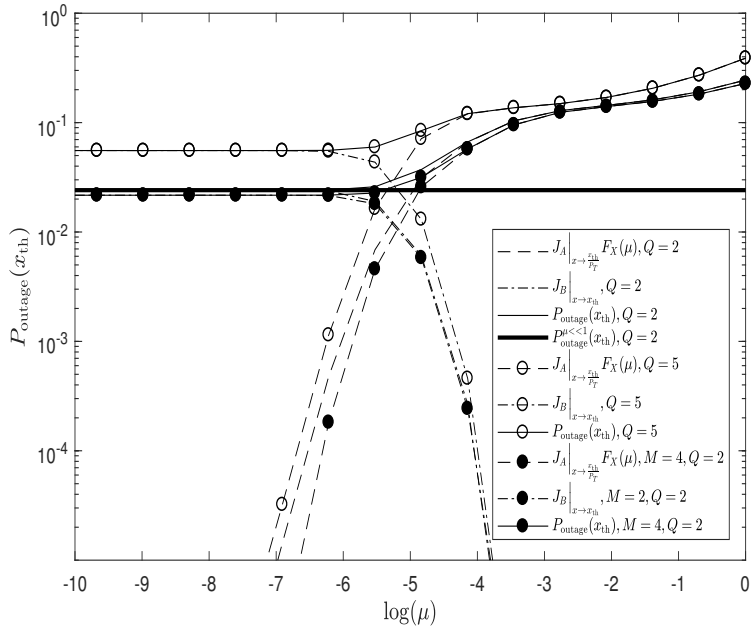

Fig. 8. Impact of μ on $P_{\text{outage}}(x_{\text{th}})$ for various values of Q and M.

V. Conclusions

In this paper, we have investigated the performance improvement of the secondary users' network for cooperative spectrum sharing systems. As a transmit diversity scheme, the dCDD protocol has been employed between the transmitting side of the secondary users' network consisting of the CU, multiple S-RRHs, and a single SRX. From the performance analysis, it can be concluded that dCDD can provide a better outage probability over the existing work, which uses only one S-RRH as the secondary user transmitter due to ISI-free reception at the SRX. It has been shown that the primary users channel and system configuration parameters have no impacts when the ratio of the interference temperature to the maximum transmission power is constant on the outage probability. However, as this ratio decreases, the outage probability of the considered spectrum sharing system has shown to be limited by the outage probability floor.

Appendix A: Computation of the distribution of the RV Y

We can see that $F_{A,\text{L}}(x)$ is proportional to a term $e^{-\frac{x}{\alpha_{h,\text{L}}}}x^k$ for $k \in \mathbb{N}_0$. In addition, $f_B(x|d_2)$ is expressed by a mixture of two parts, each of which is independent of each other. Thus, we will mainly focus on the computation related with the first LoS-relevant part, which is somewhat similar to those of [39].

The conditional probability, $P_r(Y < x|d_2)$, is given by

$$P_r(Y < x|d_2) \propto \int_0^\infty e^{-\frac{xy}{\alpha_{h,\text{L}}}}(xy)^k f_B(y|d_2)dy$$

$$= \frac{x^k \Gamma(k+\hat{N}_{\mathrm{L}})(P_p)^k (d_2)^{\epsilon_{\mathrm{L}}\hat{N}_{\mathrm{L}}}}{\Gamma(\hat{N}_{\mathrm{L}})} \left(\frac{P_p x}{\alpha_{h,\mathrm{L}}} + d_2^{\epsilon_{\mathrm{L}}}\right)^{-k-\hat{N}_{\mathrm{L}}}. \tag{A.1}$$

From (A.1), $P_r(Y<x)$ is computed as follows:

$$P_r(Y<x) \propto \int_{R_{\min}}^{R} P_r(Y<x|z) f_{d_2}(z) dz. \tag{A.2}$$

Now applying (3), we can have

$$\begin{aligned} P_r(Y<x) &\propto \int_{R_{\min}}^{R} \frac{x^k \Gamma(k+\hat{N}_{\mathrm{L}})(P_p)^k (z)^{\epsilon_{\mathrm{L}}\hat{N}_{\mathrm{L}}+1}}{\Gamma(\hat{N}_{\mathrm{L}})} \left(\frac{P_p x}{\alpha_{h,\mathrm{L}}} + z^{\epsilon_{\mathrm{L}}}\right)^{-k-\hat{N}_{\mathrm{L}}} dz \\ &= \frac{\Gamma(k+\hat{N}_{\mathrm{L}})}{\Gamma(\hat{N}_{\mathrm{L}})} \frac{(P_p)^{-\hat{N}_{\mathrm{L}}}(\alpha_{h,\mathrm{L}})^{k+\hat{N}_{\mathrm{L}}}}{\epsilon_{\mathrm{L}}\mu_{\mathrm{L}}} x^{-\hat{N}_{\mathrm{L}}} \Bigg[(R)^{\epsilon_{\mathrm{L}}\mu_{\mathrm{L}}} \cdot {}_2F_1\Big(\mu_{\mathrm{L}}, k+\hat{N}_{\mathrm{L}}; \mu_{\mathrm{L}}+1; -\frac{(R)^{\epsilon_{\mathrm{L}}}\alpha_{h,\mathrm{L}}}{P_p x}\Big) - \\ &\quad (R_{\min})^{\epsilon_{\mathrm{L}}\mu_{\mathrm{L}}} \cdot {}_2F_1\Big(\mu_{\mathrm{L}}, k+\hat{N}_{\mathrm{L}}; \mu_{\mathrm{L}}+1; -\frac{(R_{\min})^{\epsilon_{\mathrm{L}}}\alpha_{h,\mathrm{L}}}{P_p x}\Big) \Bigg] \\ &= \frac{\Gamma(k+\hat{N}_{\mathrm{L}})}{\Gamma(\hat{N}_{\mathrm{L}})} \frac{(P_p)^{-\hat{N}_{\mathrm{L}}}(\alpha_{h,\mathrm{L}})^{k+\hat{N}_{\mathrm{L}}}}{\epsilon_{\mathrm{L}}\mu_{\mathrm{L}}} x^{-\hat{N}_{\mathrm{L}}} \mathbb{A}_{\mathrm{L},1} \end{aligned} \tag{A.3}$$

where [40, Eq. (2.10.3.2)] is used in this derivation. Having applied the derivation for different cases and some manipulations, we can derive Theorem 1.

Appendix B: Derivation of Corollary 4

We mainly use the term $x^{-\hat{N}_{\mathrm{L}}}\mathbb{A}_{\mathrm{L},\mathrm{L}}$ specified in (20). That is, we can have (B.1) as follows:

$$\begin{aligned} \mathbb{D}_{\mathrm{L},\mathrm{L}} = \int_0^{\infty} t^{-\hat{N}_{\mathrm{L}}} \Bigg[R^{\mu_{\mathrm{L}}\epsilon_{\mathrm{L}}} \underbrace{{}_2F_1\Big(\mu_{\mathrm{L}}, k+\hat{N}_{\mathrm{L}}; \mu_{\mathrm{L}}+1; -\frac{I_p(R)^{\epsilon_{\mathrm{L}}}\alpha_{h,\mathrm{L}}}{P_p x t}\Big)}_{J_2} - \\ (R_{\min})^{\mu_{\mathrm{L}}\epsilon_{\mathrm{L}}} {}_2F_1\Big(\mu_{\mathrm{L}}, k+\hat{N}_{\mathrm{L}}; \mu_{\mathrm{L}}+1; -\frac{I_p(R_{\min})^{\epsilon_{\mathrm{L}}}\alpha_{h,\mathrm{L}}}{P_p x}\Big) \Bigg] \Upsilon \Big[\underbrace{\tilde{l} e^{-\tilde{\beta}t} t^{\tilde{l}-1}}_{J_3} - \tilde{\beta} e^{-\tilde{\beta}t} t^{\tilde{l}} \Big] dt. \end{aligned} \tag{B.1}$$

Let us focus on the computation relevant to J_2 and J_3 as follows:

$$\begin{aligned} \mathbb{D}_{\mathrm{L},\mathrm{L}} &\propto \tilde{l} \int_0^{\infty} t^{-\hat{N}_{\mathrm{L}}} {}_2F_1\Big(\mu_{\mathrm{L}}, k+\hat{N}_{\mathrm{L}}; \mu_{\mathrm{L}}+1; -\frac{I_p(R)^{\epsilon_{\mathrm{L}}}\alpha_{h,\mathrm{L}}}{P_p x t}\Big) e^{-\tilde{\beta}t} t^{\tilde{l}-1} dt \\ &= \tilde{l} \frac{\Gamma(\mu_{\mathrm{L}}+1)}{\Gamma(\mu_{\mathrm{L}})\Gamma(k+\hat{N}_{\mathrm{L}})} \int_0^{\infty} t^{-\hat{N}_{\mathrm{L}}+\tilde{l}-1} e^{-\tilde{\beta}t} G_{2,2}^{2,1}\left(\frac{P_p x t}{I_p(R)^{\epsilon_{\mathrm{L}}}\alpha_{h,\mathrm{L}}} \middle| \begin{matrix} 1, \mu_{\mathrm{L}}+1 \\ \mu_{\mathrm{L}}, k+\hat{N}_{\mathrm{L}} \end{matrix} \right) dt \\ &= \tilde{l} \frac{\Gamma(\mu_{\mathrm{L}}+1)}{\Gamma(\mu_{\mathrm{L}})\Gamma(k+\hat{N}_{\mathrm{L}})} (\tilde{\beta})^{\hat{N}_{\mathrm{L}}-\tilde{l}} G_{3,2}^{2,2}\left(\frac{P_p x}{I_p(R)^{\epsilon_{\mathrm{L}}}\alpha_{h,\mathrm{L}}\tilde{\beta}} \middle| \begin{matrix} 1+\hat{N}_{\mathrm{L}}-\tilde{l}, 1, \mu_{\mathrm{L}}+1 \\ \mu_{\mathrm{L}}, k+\hat{N}_{\mathrm{L}} \end{matrix} \right) \end{aligned} \tag{B.2}$$

where we have used [38, eq. (07.34.22.0003.01)], [41, eq. (2.24.3.1)]. Thus, we can have the following form for $\mathbb{D}_{\mathrm{L},\mathrm{L}}$.

$$\begin{aligned} \mathbb{D}_{\mathrm{L},\mathrm{L}} = \Upsilon \Bigg[\frac{\tilde{l}(R)^{\mu_{\mathrm{L}}\epsilon_{\mathrm{L}}}\Gamma(\mu_{\mathrm{L}}+1)(\tilde{\beta})^{\hat{N}_{\mathrm{L}}-\tilde{l}}}{\Gamma(\mu_{\mathrm{L}})\Gamma(k+\hat{N}_{\mathrm{L}})} G_{3,2}^{2,2}\left(\frac{P_p x}{I_p(R)^{\epsilon_{\mathrm{L}}}\alpha_{h,\mathrm{L}}\tilde{\beta}} \middle| \begin{matrix} 1+\hat{N}_{\mathrm{L}}-\tilde{l}, 1, \mu_{\mathrm{L}}+1 \\ \mu_{\mathrm{L}}, k+\hat{N}_{\mathrm{L}} \end{matrix} \right) - \\ \frac{(R_{\min})^{\mu_{\mathrm{L}}\epsilon_{\mathrm{L}}}\Gamma(\mu_{\mathrm{L}}+1)(\tilde{\beta})^{\hat{N}_{\mathrm{L}}-\tilde{l}}}{\Gamma(\mu_{\mathrm{L}})\Gamma(k+\hat{N}_{\mathrm{L}})} G_{3,2}^{2,2}\left(\frac{P_p x}{I_p(R_{\min})^{\epsilon_{\mathrm{L}}}\alpha_{h,\mathrm{L}}\tilde{\beta}} \middle| \begin{matrix} \hat{N}_{\mathrm{L}}-\tilde{l}, 1, \mu_{\mathrm{L}}+1 \\ \mu_{\mathrm{L}}, k+\hat{N}_{\mathrm{L}} \end{matrix} \right) \Bigg]. \end{aligned} \tag{B.3}$$

Based on (B.3), the following terms can be readily derived as:

$$\mathbb{D}_{\mathrm{L,nL}} = \mathbb{D}_{\mathrm{L,L}}\Big|_{\epsilon_{\mathrm{L}}\to\epsilon_{\mathrm{nL}},\mu_{\mathrm{L}}\to\mu_{\mathrm{nL}},\hat{N}_{\mathrm{L}}\to\hat{N}_{\mathrm{nL}}},\ \mathbb{D}_{\mathrm{nL,L}} = \mathbb{D}_{\mathrm{L,L}}\Big|_{\alpha_{h,\mathrm{L}}\to\alpha_{h,\mathrm{nL}}},\ \text{and}$$
$$\mathbb{D}_{\mathrm{nL,nL}} = \mathbb{D}_{\mathrm{L,L}}\Big|_{\alpha_{h,\mathrm{L}}\to\alpha_{h,\mathrm{nL}},\epsilon_{\mathrm{L}}\to\epsilon_{\mathrm{nL}},\mu_{\mathrm{L}}\to\mu_{\mathrm{nL}},\hat{N}_{\mathrm{L}}\to\hat{N}_{\mathrm{nL}}}. \tag{B.4}$$

In (B.3), $G_{p,q}^{m,n}\left(t\left|\begin{array}{c} a_1,...,a_n,a_{n+1},...,a_p \\ b_1,...,b_m,b_{m+1},...,b_q \end{array}\right.\right)$ denotes the Meijer G-function [37, Eq. (9.301)].

REFERENCES

[1] K. J. Kim, H. Liu, M. D. Renzo, and H. V. Poor, "Performance analysis of spectrum sharing systems with distributed CDD," in *Proc. 2018 IEEE GLOBECOM*, Abu Dhabi, UAE, Dec. 2018, pp. 1–6.

[2] J. Mitola and G. Q. Maguire, "Cognitive radios: Making software radios more personal," *IEEE Personal Commun. Mag.*, vol. 6, pp. 13–18, Aug. 1999.

[3] T. K. Y. Lo, "Maximum ratio transmission," *IEEE Trans. Commun.*, vol. 47, no. 10, pp. 1458–1461, Oct. 1999.

[4] K. J. Kim, T. Khan, and P. Orlik, "Performance analysis of cooperative systems with unreliable backhauls and selection combining," *IEEE Trans. Veh. Technol.*, vol. 66, no. 3, pp. 2448–2461, Mar. 2017.

[5] V. M. Blagojevic and P. N. Ivanis, "Ergodic capacity for TAS/MRC spectrum sharing cognitive radio," *IEEE Commun. Lett.*, vol. 16, no. 3, pp. 312–323, Mar. 2012.

[6] P. L. Yeoh, M. Elkashlan, T. Q. Trung, N. Yang, and D. B. da Costa, "Transmit antenna selection for interference management in cognitive relay networks," *IEEE Trans. Veh. Technol.*, vol. 63, no. 7, pp. 3250–3262, 2014.

[7] K. Tourki, F. A. Khan, K. A. Qaraqe, H. C. Yang, and M. S. Alouini, "Exact performance analysis of MIMO cognitive radio systems using transmit antenna selection," *IEEE J. Sel. Areas Commun.*, vol. 32, no. 3, pp. 425–438, Mar. 2014.

[8] M. Hanif, H. C. Yang, and M. S. Alouini, "Transmit antenna selection for power adaptive underlay cognitive radio with instantaneous interference constraint," *IEEE Trans. Commun.*, vol. 65, no. 6, pp. 2357–2367, Jun. 2017.

[9] H. Pennanen, A. Tlli, and M. Latva-aho, "Multi-cell beamforming with decentralized coordination in cognitive and cellular networks," *IEEE Trans. Signal Process.*, vol. 62, no. 2, pp. 295–308, Jan. 2014.

[10] G. Zheng, Z. Ho, E. A. Jorswieck, and B. Ottersten, "Information and energy cooperation in cognitive radio networks," *IEEE Trans. Signal Process.*, vol. 62, no. 9, pp. 2290–2303, May 2014.

[11] H. T. Nguyen, T. Q. Duong, and W. J. Hwang, "Multiuser relay networks over unreliable backhaul links under spectrum sharing environment," *IEEE Commun. Lett.*, vol. 21, no. 10, pp. 2314–2317, Oct. 2017.

[12] S. Lee, J. Kang, S. Jeong, J. Kang, and S. Al-Araji, "Joint design of precoder and backhaul quantizer in cooperative cognitive radio networks," *IEEE Trans. Veh. Technol.*, vol. 66, no. 2, pp. 1871–1875, 2017.

[13] K. J. Kim, M. D. Renzo, H. Liu, P. V. Orlik, and H. V. Poor, "Performance analysis of distributed single carrier systems with distributed cyclic delay diversity," *IEEE Trans. Commun.*, vol. 65, no. 12, pp. 5514–5528, Dec. 2017.

[14] Y.-C. Liang, W. S. Leon, Y. Zeng, and C. Xu, "Design of cyclic delay diversity for single carrier cyclic prefix (SCCP) transmissions with block-iterative GDFE (BI-GDFE) receiver," *IEEE Trans. Wireless Commun.*, vol. 7, no. 2, pp. 677–684, Feb. 2008.

[15] A. H. Mehana and A. Nosratinia, "Single-carrier frequency-domain equalizer with multi-antenna transmit diversity," *IEEE Trans. Wireless Commun.*, vol. 12, pp. 388–397, Jan. 2013.

[16] Q. Li, Q. Yan, K. C. Keh, K. H. Li, and Y. Hu, "A multi-relay-selection scheme with cyclic delay diversity," *IEEE Commun. Lett.*, vol. 17, no. 2, pp. 349–352, Feb. 2013.

[17] U.-K. Kwon and G.-H. Im, "Cyclic delay diversity with frequency domain turbo equalization for uplink fast fading channels," *IEEE Commun. Lett.*, vol. 13, no. 3, pp. 184–186, Mar. 2009.

[18] K. J. Kim and T. A. Tsiftsis, "On the performance of cyclic prefix-based single-carrier cooperative diversity systems with best relay selection," *IEEE Trans. Wireless Commun.*, vol. 10, no. 4, pp. 1269–1279, Apr. 2011.

[19] K. J. Kim, T. A. Tsiftsis, and H. V. Poor, "Power allocation in cyclic prefixed single-carrier relaying systems," *IEEE Trans. Wireless Commun.*, vol. 10, no. 7, pp. 2297–2305, Jul. 2011.

[20] K. J. Kim, T. Q. Duong, and H. V. Poor, "Outage probability of single-carrier cooperative spectrum sharing systems with decode-and-forward relaying and selection combining," *IEEE Trans. Wireless Commun.*, vol. 12, no. 2, pp. 806–817, Feb. 2013.

[21] K. J. Kim, L. Wang, T. Q. Duong, M. Elkashlan, and H. V. Poor, "Cognitive single-carrier systems: Joint impact of multiple licensed transceivers," *IEEE Trans. Wireless Commun.*, vol. 13, no. 12, pp. 6741–6755, Dec. 2014.

[22] Y. Deng, K. J. Kim, T. Q. Duong, M. Elkashlan, G. K. Karagiannidis, and A. Nallanathan, "Full-duplex spectrum sharing in cooperative single carrier systems," *IEEE Trans. on Cogn. Commun. Netw.*, vol. 2, no. 1, pp. 68–82, Mar. 2016.

[23] K. J. Kim, T. Q. Duong, H. V. Poor, and L. Shu, "Performance analysis of cyclic prefixed single-carrier spectrum sharing relay systems in primary user interference," *IEEE Trans. Signal Process.*, vol. 60, no. 12, pp. 6729–6734, Dec. 2012.

[24] X. Zhang and J. G. Andrew, "Downlink cellular network analysis with multi-slope path loss models," *IEEE Trans. Commun.*, vol. 63, no. 5, pp. 1881–1894, May 2015.

[25] T. Bai, R. Vaze, and R. W. Heath, "Analysis of blockage effects on urban cellular networks," *IEEE Trans. Wireless Commun.*, vol. 9, no. 13, pp. 5070–5083, Sep. 2014.

[26] M. Ding, P. Wang, D. Lopez-Perez, G. Mao, and Z. Lin, "Performance impact of LoS and NLoS transmissions in dense cellular networks," *IEEE Trans. Wireless Commun.*, vol. 15, no. 3, pp. 2365–2380, Mar. 2016.

[27] 3GPP, TR 36.828 (V11.0.0), "Further enhancements to LTE time division duplex (TDD) for downlink-uplink (DL-UL) interference management and traffic adaptation," Jun. 2012.

[28] C. M. Lo and W. H. Lam, "Performance of generalized selection combining for mobile radio communications with mixed cochannel interferers," *IEEE Trans. Veh. Technol.*, vol. 51, no. 1, pp. 114–121, Jan. 2002.

[29] Y. Zeng and T. S. Ng, "Pilot cyclic prefixed single carrier communication: channel estimation and equalization," *IEEE Signal Process. Lett.*, vol. 12, no. 1, pp. 56–59, Jan. 2005.

[30] F. Gao, A. Nallanathan, and C. Tellambura, "Blind channel estimation for cyclic-prefixed single-carrier systems by exploiting real symbol characteristics," *IEEE Trans. Veh. Technol.*, vol. 56, no. 5, pp. 2487–2498, Sep. 2007.

[31] H. Zhang, Y. Dong, J. Cheng, M. J. Hossain, and V. C. M. Leung, "Fronthauling for 5G LTE-U ultra dense cloud small cell networks," *IEEE Wireless Communications*, vol. 23, no. 6, pp. 48–53, Dec. 2016.

[32] X. Zhao, X. Zhou, X. Jin, and B. Xu, "Channel estimation for high speed Macro-MIMO RRH LTE-R systems in LOS and NLOS environments," in *Proc. 2018 IEEE Vehicular Technology Conference (VTC-Spring)*, Porto, Portugal, 36 Jun. 2018, pp. 1–5.

[33] P. Cardieri, "Modeling interference in wireless Ad Hoc networks," *IEEE Commun. Surveys Tuts.*, vol. 12, no. 4, pp. 551–572, Fourth Quarter 2010.

[34] A. Ghasemi and E. S. Sousa, "Fundamental limits of spectrum-sharing in fading environments," *IEEE Trans. Wireless Commun.*, vol. 6, no. 2, pp. 649–658, Feb. 2007.

[35] J. M. Peha, "Approaches to spectrum sharing," *IEEE Commun. Mag.*, vol. 43, no. 2, pp. 10–12, Feb. 2005.

[36] K. J. Kim, Y. Yue, R. A. Iltis, and J. D. Gibson, "A QRD-M/Kalman Filter-based detection and channel estimation algorithm for MIMO-OFDM systems," *IEEE Trans. Wireless Commun.*, vol. 4, pp. 710–721, Mar. 2005.

[37] I. S. Gradshteyn and I. M. Ryzhik, *Table of Integrals, Series, and Products*. New York: Academic Press, 2007.

[38] Wolfman Research Inc. Accessed: Nov.28, 2018. [Online]. Available: http://functions.wolfman.com

[39] K. J. Kim, P. V. Orlik, and T. A. Khan, "Performance analysis of finite-sized co-operative systems with unreliable backhauls," *IEEE Trans. Wireless Commun.*, vol. 15, no. 7, pp. 5001–5015, Jul. 2016.

[40] A. P. Prudnikov, Y. A. Brychkov, and O. I. Marichev, *Special Functions*, 3rd ed. London: Gordon and Breach, 1992.

[41] ——, *Integral and Series. Vol. 3: More Special Functions*, 3rd ed. London: Gordon and Breach, 1992.